Wave-induced longitudinal vortices in a shallow current

By ZHENHUA HUANG[1] AND CHIANG C. MEI[2]

[1]Department of Civil Engineering, The Hong Kong University of Science and Technology,
Clearwater Bay, Hong Kong, PR China

[2]Department of Civil and Environmental Engineering, Massachusetts Institute of Technology,
Cambridge MA, 02139, USA

An instability theory is presented for the initiation of longitudinal vortices due to waves interacting with a turbulent current in an open channel of finite depth. With a simple model of eddy viscosity the dimensionless shearing rate of the basic current is much weaker than the dimensionless velocity almost everywhere except near the bed. We shall show that in addition to the internal vortex force, a mean shear stress exists on the mean sea level, owing to nonlinear wave–current interactions, despite the absence of wind. This stress adds vertical vorticity to the interior and augments the vortex force mechanism of instability significantly. Effects of current strength and wave conditions on the unstable growth are studied by numerical examples.

1. Introduction

Wind-induced horizontal vortices first observed in a large lake by Langmuir (1938) are an important subject of air–sea interactions. A comprehensive survey of the earlier observations and theories have been given by Leibovich (1983). Field data in the deep sea by Weller *et al.* (1985), Smith, Pinkel & Weller (1987), Weller & Price (1998), Smith (1992), Li, Zahariev & Garrett (1995) and Graham & Hall (1997) have established that Langmuir circulation is responsible for the deepening of the surface mixed layer and the rapid erosion of the thermoclines.

There are only a few laboratory studies of horizontal vortices in waves and currents. Faller & Caponi (1978) were the first to investigate the wind-induced circulation in a shallow tank. Without wind, Nepf & Monismith (1991) also found similar circulations for mechanically generated waves riding on an open-channel flow over a smooth bottom. Their waves were very short ($kh \approx 9$) so that the bottom did not affect the cells. Nepf *et al.* (1995) also investigated the influence of breaking waves. In both experiments, the tank width was small enough for sidewall effects to be felt. In flume experiments of waves on a current over a rough bed, Klopman (1997) also found circulations, again strongly affected by sidewalls. Melville, Shear & Veron (1998) investigated Langmuir cells due to wind-generated waves and current. Attention was focused on the early events near the sea surface, when both current and waves were still in the process of development.

On the theoretical side, an important mechanism has been advanced by Craik & Leibovich (1976), Craik (1977), Leibovich (1977, 1983), etc. Neglecting the direct effects of wind and assuming the wind-induced drift to be as weak as the wave-induced Stokes drift, they found that an internal 'vortex force' is responsible for the formation of Langmuir circulation through instability (the CL-II theory). In

particular, a necessary condition for instability is that somewhere in the water column

$$\frac{\partial U_s}{\partial z} \frac{\partial U_0}{\partial z} > 0, \tag{1.1}$$

where U_s is the Stokes drift velocity and U_0 the wind-induced current. Craik (1982a) pointed out that for pure waves, the Langmuir circulation is possible because of the wave-induced drift current. Extensions of the CL-II theory to include nonlinear effects in stratified and non-stratified deep ocean have been reported by Leibovich (1977b), Leibovich & Radhakrishnan (1977), Leibovich & Paolucci (1981), Skyllingstad & Denbo (1995), Gnanadesikan (1996), Li & Garrett (1997), Phillips (2001), and others. Dingemans *et al.* (1996) and Groeneweg & Battjes (2003) investigated the effects of the longitudinal vorticity on the mean current in a channel. Phillips (2002) studied the effect of the growing and decaying waves on the Langmuir circulation in deep sea. Chini & Leibovich (2003) studied the interaction between the Langmuir circulation and internal waves. A review of these theories and related observations has been given by Thorpe (2004).

Craik (1982b) also made extensions of the linear instability theory for a moderately strong current where the velocity can be of the order $O(\epsilon C)$ or $O(C)$ with ϵ being the wave slope and C the wave phase speed. Phillips (1998) extended Craik's theory to include viscosity and nonlinearity. In these studies, the dimensionless shearing rate of the current is of the same order as the velocity as the vertical length scale is comparable to the characteristic wavelength.

Langmuir vortices have been observed in shallow lakes (Szeri 1996). These circulations can be of importance to the transport of suspended sediments which are often carriers of nutrients or toxic wastes. Motivated by such environmental interests, we analyse below one of the possible alternative sources of longitudinal vortices in shallow water, i.e. interactions between waves and an open-channel current maintained by river flow or tides, without wind. This type of current has two features distinct from the drift current forced by wind. First, the velocity shear is the strongest near the seabed, not near the free surface as in a drift current forced by wind. Secondly, in most of the flow, the dimensionless velocity shear is much weaker than the dimensionless velocity itself.

Extending the two-dimensional theory of Huang & Mei (2003) to three dimensions, we adopt a depth-dependent eddy-viscosity model and assume that turbulence is dominated by the current. The linearized equations, now involving the slope and curvature of the eddy viscosity, is similar to the CL-II thoery so that the mechanism of internal vortex force still applies. However, we shall show that there is a mean shear stress on the mean sea surface, so far unaccounted for, owing to interactions between waves and the background current, despite the absence of wind. This new surface stress feeds vertical vorticity downward and produces additional longitudinal vorticity via the current shear, and hence amplifies the CL-II mechanism. Numerical solutions show that longitudinal vortices can be formed in both wave-following and wave-opposing currents. The effects of wave slope, current strength and the cell spacing on the growth rate of vortices are studied by numerical examples. Various components of mechanical energy are compared to see their contributions to the total growth rate.

2. Governing equations and boundary conditions

2.1. *Assumptions and Reynolds equations*

We focus our interest on the effects of waves on a pre-existing turbulent current whose velocity is as strong as the orbital velocity of waves. For simplicity, only a

smooth bed is considered here so that modification of the current by waves in the bottom wave boundary layer is not important (for a rough seabed, turbulence in the bottom boundary layer can be enhanced, Grant & Madsen 1986). We shall employ a simple model of depth-varying eddy viscosity which was used by Huang & Mei (2003) to explain the observed two-dimensional phenomenon that the current velocity is increased (decreased) near the free surface if followed (opposed) by waves (Kemp & Simons 1982, 1983; Klopman 1997).

Following an idea due to Townsend (1972) and used also by Van Duin & Janssen (1992) in their studies of wind flow over a wavy sea surface, we shall assume that the total effective viscosity ν_T^* is the sum of molecular viscosity ν and a depth-dependent eddy viscosity ν_e^* which vanishes at the seabed and at the moving sea surface $z^* = \eta^*$,

$$\nu_T^* = \nu + \nu_e^*, \quad \nu_e^* = \kappa u_f (-z^* + \eta^*)\left(1 + \frac{z^*}{h}\right), \quad z_B^* - h < z^* < \eta^*, \tag{2.1}$$

with u_f being the friction velocity characterizing the current strength, $\kappa = 0.4$ the Kármán constant, h the water depth. In the uniform open-channel flow with $\eta^* = 0$, (2.1) leads to a logarithmic velocity profile. The height z_B^* is the empirical hydraulic roughness for a smooth bed signifying the apparent bottom where the logarithmic velocity vanishes.

Let us normalize all space coordinates by the inverse of the wavenumber k, time by the inverse of the wave frequency ω, velocity by the wave phase velocity $C = \omega/k$, and the dynamic pressure and Reynolds stresses by ρC^2, i.e.

$$\left.\begin{array}{c} (x_1, x_2, x_3) \equiv k(x_1^*, x_2^*, x_3^*), \quad t = \omega t^*, \\[2mm] \eta = k\eta^*, \quad \boldsymbol{q} \equiv (q_1, q_2, q_3) \equiv \dfrac{\boldsymbol{q}^*}{C}, \quad p = \dfrac{p^*}{\rho C^2}, \quad \tau_{ij} = \dfrac{\tau_{ij}^*}{\rho C^2}, \end{array}\right\} \tag{2.2}$$

where η^* is the instantaneous free-surface displacement, $(x_1, x_2, x_3) \equiv (x, y, z)$ and $(q_1, q_2, q_3) = (u, v, w)$. All physical variables are marked with asterisks and their normalized counterparts without. In dimensionless form, the laws of conservation of mass and momentum are

$$\nabla \cdot \boldsymbol{q} = 0 \tag{2.3}$$

$$\frac{\partial \boldsymbol{q}}{\partial t} + (\boldsymbol{q} \cdot \nabla)\boldsymbol{q} + \nabla p = \nabla \cdot \boldsymbol{T} \tag{2.4}$$

where $\boldsymbol{T} \equiv \{\tau_{ij}\}$ is the dimensionless Reynolds stress tensor.

Normalized by $\omega/k^2 = C/k$, i.e. $\nu_T^* = C\nu/k$, the dimensionless total viscosity ν_T is

$$\nu_T = \frac{k\nu}{C} + \nu_e = \frac{k\nu}{C} + \kappa \frac{u_f}{C}[\bar{S}(z) + \eta \hat{S}(z)], \quad -kh + z_b < z < \eta, \tag{2.5}$$

where $z_b = kz_B^*$ is the dimensionless hydraulic roughness, and

$$\bar{S} = -z\left(1 + \frac{z}{kh}\right), \quad \hat{S} = 1 + \frac{z}{kh} \tag{2.6}$$

are the profile factors of the steady and wave-induced parts of the eddy viscosity, respectively. We stress that the friction velocity u_f includes the two-dimensional modification by waves and can be calculated by the theory of Huang & Mei (2003).

We next assume that (i) the dimensionless water depth is of order unity, $kh = O(1)$, (ii) the wave steepness is small, $\epsilon = ka \ll 1$, and (iii) the wave orbital velocity is comparable to the current velocity. Now the problem involves two parameters, the current strength parameter u_f/C and the wave steepness ϵ signifying nonlinearity. Under

typical laboratory and field conditions u_f/C has been estimated by Huang & Mei (2003) to be about $O(0.002 \sim 0.01)$. For ordering convenience we shall take $u_f/C = O(\epsilon^2)$ and write

$$\kappa \frac{u_f}{C} = \alpha \epsilon^2 \quad \text{with } \alpha = O(1). \tag{2.7}$$

For brevity, the total viscosity will be denoted by

$$\nu_T = \epsilon^2 S_T(z, \eta) \equiv \epsilon^2 [C_s + \alpha(\bar{S}(z) + \eta \hat{S}(z))] \text{ with } C_s \equiv \frac{k\nu}{\epsilon^2 C} = \frac{\nu}{\omega a^2}. \tag{2.8}$$

As a preliminary estimate, for waves of a period $2\pi/\omega = 6.28$ s, we find $C_s = 10^{-4}$ if $a = 0.1$ m and $C_s = 10^{-6}$ if $a = 1$ m. Thus, ν_T is dominated by the eddy viscosity almost everywhere except on the free surface where only molecular viscosity remains. Near the seabed, the molecular viscosity can be discarded and a hydraulic roughness z_b will be introduced to avoid the logarithmic singularity. The factor α is a measure of the relative importance of the current to waves, and represents physically the ratio of the rate of vorticity diffusion to the rate of vorticity production by waves in the wave–current system, similar to the Langmuir number in Leibovich (1977a).

In terms of S_T, the Reynolds stress components can be written as

$$\tau_{xx} = 2\epsilon^2 S_T \frac{\partial u}{\partial x}, \quad \tau_{yy} = 2\epsilon^2 S_T \frac{\partial v}{\partial y}, \quad \tau_{zz} = 2\epsilon^2 S_T \frac{\partial w}{\partial z}, \tag{2.9a}$$

$$\tau_{xy} = \epsilon^2 S_T \left(\frac{\partial u}{\partial y} + \frac{\partial v}{\partial x}\right), \quad \tau_{xz} = \epsilon^2 S_T \left(\frac{\partial u}{\partial z} + \frac{\partial w}{\partial x}\right), \quad \tau_{zy} = \epsilon^2 S_T \left(\frac{\partial w}{\partial y} + \frac{\partial v}{\partial z}\right). \tag{2.9b}$$

Let the vorticity $\boldsymbol{\Omega}$ be defined by

$$\boldsymbol{\Omega} = (\xi, \vartheta, \zeta) = \nabla \times \boldsymbol{q}. \tag{2.10}$$

For later use, we rewrite the momentum equation (2.4) as

$$\frac{\partial \boldsymbol{q}}{\partial t} + \nabla p = -\nabla E + \boldsymbol{q} \times \boldsymbol{\Omega} + \nabla \cdot \boldsymbol{T} \quad \text{where} \quad E = \tfrac{1}{2}\boldsymbol{q} \cdot \boldsymbol{q}. \tag{2.11}$$

By taking the curl of (2.11), the vorticity transport equation is obtained

$$\frac{\partial \boldsymbol{\Omega}}{\partial t} = -(\boldsymbol{q} \cdot \nabla)\boldsymbol{\Omega} + (\boldsymbol{\Omega} \cdot \nabla)\boldsymbol{q} + \nabla \times (\nabla \cdot \mathbf{T}). \tag{2.12}$$

2.2. *Boundary conditions*

On the sea bottom, we follow the usual practice in open-channel flows and introduce the hydraulic roughness z_b representing the apparent bottom where there is no slip

$$u = v = w = 0, \quad z = -kh + z_b. \tag{2.13}$$

On the moving free surface, the kinematic boundary condition is

$$\frac{\partial \eta}{\partial t} + q_j \frac{\partial \eta}{\partial x_j} - w = 0, \quad j = 1, 2, \quad z = \eta, \tag{2.14}$$

where the indices $j = 1, 2$ refer to the horizontal coordinates only and summation over the repeated index j is implied. The normalized dynamic surface boundary conditions are

$$\tau_{i3} = [-(p - \coth(kh)\eta)\delta_{ij} + \tau_{ij}]\frac{\partial \eta}{\partial x_j} + (p - \coth(kh)\eta)\delta_{i3} \, (i = 1, 2, 3), \tag{2.15}$$

where p is the dimensionless dynamic pressure (see for example, Mei 1989). The well-known dispersion relation $\omega^2 = gk \tanh kh$ of the first-order waves has been used here.

Treating the oscillatory boundary layer on the free surface is involved since the boundary-layer thickness can be much smaller than the wave amplitude. Instead, we shall integrate the continuity and momentum equations from the moving surface $z = \eta$ downward, in order to transfer these free-surface conditions to the level $z = 0$. This approach has been used before by Liu & Davis (1977) in studying the wave-induced mass transport in two dimensions (their solution has a singularity which has been resolved by Craik 1982a.) and is similar to the derivation of depth-integrated time-averaged equations leading to the radiation stresses (see, e.g. Mei 1989).

2.2.1. *Exact boundary conditions at $z = 0$*

Integrating the continuity equation (2.3) from $z = 0$ to $z = \eta$, making use of Leibniz's rule and applying the surface boundary condition (2.14), we obtain

$$\frac{\partial \eta}{\partial t} + \frac{\partial}{\partial x_j} \int_0^\eta q_j \, \mathrm{d}z - [w]_0 = 0 \quad j = 1, 2, \tag{2.16}$$

which is exact, and will be regarded as the kinematic boundary condition on $z = 0$.

Next, we derive the normal stress condition. Integrating the vertical component of the momentum equation (2.4) from $z = 0$ to $z = \eta$, we have

$$\int_0^\eta \frac{\partial w}{\partial t} \, \mathrm{d}z + \int_0^\eta \frac{\partial q_j w}{\partial x_j} \, \mathrm{d}t + [ww]_\eta - [ww]_0 + [p]_\eta - [p]_0$$
$$= \int_0^\eta \frac{\partial \tau_{3j}}{\partial x_j} \, \mathrm{d}z + [\tau_{33}]_\eta - [\tau_{33}]_0. \tag{2.17}$$

After using Leibniz's identity and applying the kinematic boundary condition (2.14), we obtain

$$\frac{\partial}{\partial t} \int_0^\eta w \, \mathrm{d}z + \frac{\partial}{\partial x_j} \int_0^\eta q_j w \, \mathrm{d}t - [w^2]_0 + [p]_\eta - [p]_0$$
$$= \frac{\partial}{\partial x_j} \int_0^\eta \tau_{3j} \, \mathrm{d}z - [\tau_{3j}]_\eta \frac{\partial \eta}{\partial x_j} + [\tau_{33}]_\eta - [\tau_{33}]_0 \tag{2.18}$$

Equation (2.15) can be used in (2.18) to eliminate $[\tau_{33}]_\eta$, giving

$$[\tau_{33}]_0 = [p]_0 - \eta \coth(kh) + \frac{\partial}{\partial x_j} \int_0^\eta \tau_{3j} \, \mathrm{d}z - \frac{\partial}{\partial t} \int_0^\eta w \, \mathrm{d}z$$
$$- \frac{\partial}{\partial x_j} \int_0^\eta q_j w \, \mathrm{d}t + [ww]_0. \tag{2.19}$$

The left-hand side is related to the velocity via (2.9).

Now the tangential stress conditions. Integrating the horizontal components of the momentum equation (2.4) from $z = 0$ to $z = \eta$, we obtain

$$\int_0^\eta \frac{\partial q_i}{\partial t} \, \mathrm{d}z + \int_0^\eta \frac{\partial q_j q_i}{\partial x_j} \, \mathrm{d}z + [wq_i]_0 - [wq_i]_\eta + \int_0^\eta \frac{\partial p}{\partial x_i} \, \mathrm{d}z$$
$$= \int_0^\eta \frac{\partial \tau_{ij}}{\partial x_j} \, \mathrm{d}z + [\tau_{i3}]_0 - [\tau_{i3}]_\eta, \tag{2.20}$$

where $i = 1, 2$. After using the Leibniz's identity and the kinematic surface boundary condition (2.14) to replace the term $\partial \eta / \partial t$, we obtain

$$\frac{\partial}{\partial t} \int_0^\eta q_i \, dz + \frac{\partial}{\partial x_j} \int_0^\eta q_j q_i \, dz - [w q_i]_0 + \frac{\partial}{\partial x_i} \int_0^\eta p \, dz - [p]_\eta \frac{\partial \eta}{\partial x_i}$$
$$= \frac{\partial}{\partial x_j} \int_0^\eta \tau_{ij} \, dz - [\tau_{ij}]_\eta \frac{\partial \eta}{\partial x_j} + [\tau_{i3}]_\eta - [\tau_{i3}]_0. \quad (2.21)$$

By making use of the surface dynamic boundary condition (2.15), the shear stress $[\tau_{i3}]_\eta$ in (2.21) can be eliminated so that

$$[\tau_{i3}]_0 = -\frac{\partial}{\partial t} \int_0^\eta q_i \, dz - \frac{\partial}{\partial x_j} \int_0^\eta (q_j q_i) \, dz + [w q_i]_0$$
$$- \frac{\partial}{\partial x_i} \int_0^\eta p \, dz + \frac{\partial}{\partial x_j} \int_0^\eta \tau_{ij} \, dz + \frac{\coth(kh)}{2} \frac{\partial \eta^2}{\partial x_i} \quad i = 1, 2. \quad (2.22)$$

The left-hand side is also related to the velocity via (2.9).

Equations (2.16), (2.19) and (2.22) will be time-averaged to obtain the free-surface conditions for the current.

2.2.2. *Time-averaged shear stress at $z = 0$*

After taking the time average of (2.22) over a wave period, we obtain

$$[\bar{\tau}_{i3}]_0 = -\frac{\partial}{\partial t} \overline{\int_0^\eta q_i \, dz} - \frac{\partial}{\partial x_j} \overline{\int_0^\eta (q_j q_i) \, dz} + [\overline{w q_i}]_0$$
$$- \frac{\partial}{\partial x_i} \overline{\int_0^\eta p \, dz} + \frac{\partial}{\partial x_j} \overline{\int_0^\eta \tau_{ij} \, dz} + \frac{\coth(kh)}{2} \frac{\partial \overline{\eta^2}}{\partial x_i} \quad (i = 1, 2), \quad (2.23)$$

which is the mean tangential stress on $z = 0$. It may be emphasized that, even without wind, the mean shear stress at $z = 0$ is non-zero in general owing to the quadratic terms on the right-hand side of the preceding equation. These stress conditions on the mean surface are so far exact and hold for both laminar and turbulent flows.

Equation (2.23) states that, as a result of mean momentum balance in a fluid column between the free surface and the mean water level, there is a mean shear stress on $z = 0$, despite the absence of wind. The present approach accounts for the effects of the surface boundary layer without explicit boundary-layer analysis (Equation (2.23) can be used to examine the mass transport induced by long-crested regular waves attenuating in time. Phillips (1977) (§ 3.4) and Craik (1982*a*) employed a similar reasoning to derive the mean shear stress on the mean water surface without invoking the Stokes surface boundary layer, as did Longuet-Higgins (1953) who used a surface-conforming orthogonal coordinate system. For small-amplitude two-dimensional waves attenuating slowly in time, but not in space, only the first and third terms on the right-hand side of (2.23) are dominant. It is straightforward to reproduce the surface boundary condition in Phillips (1977) and Craik (1982*a*): $\nu [\partial \bar{u}^* / \partial z^*]_0 = 2 \nu \omega k^2 a^2 \coth kh$.)

Let us first turn to the basic state of two-dimensional flow where long-crested waves coexist with a coflowing or counterflowing turbulent current.

3. Two-dimensional basic state

Let capital symbols denote the two-dimensional basic state: $H(x, z, t)$ is the surface displacement, $P(x, z, t)$ the pressure, and (U, W) the velocity components. Denoting

the wave phase by $\theta = x - t$, the basic state including both the core and the bottom boundary layer can be formally expressed by

$$
\begin{aligned}
U = {}& \boxed{\epsilon U_0^{(1)} + \epsilon^2 U_0^{(2)} + \epsilon \left(U_1^{(1)} \mathrm{e}^{\mathrm{i}\theta} + \mathrm{c.c.} \right)} + \epsilon^2 \left(U_1^{(2)} \mathrm{e}^{\mathrm{i}\theta} + \mathrm{c.c.} \right) \\
& + \epsilon^2 \left(U_2^{(2)} \mathrm{e}^{2\mathrm{i}\theta} + \mathrm{c.c.} \right) + O(\epsilon^3),
\end{aligned}
\tag{3.1}
$$

$$
W = \boxed{\epsilon \left(W_1^{(1)} \mathrm{e}^{\mathrm{i}\theta} + \mathrm{c.c.} \right)} + \epsilon^2 \left(W_1^{(2)} \mathrm{e}^{\mathrm{i}\theta} + \mathrm{c.c.} \right) + \epsilon^2 \left(W_2^{(2)} \mathrm{e}^{2\mathrm{i}\theta} + \mathrm{c.c.} \right) + O(\epsilon^3),
\tag{3.2}
$$

$$
\begin{aligned}
P = {}& \boxed{\epsilon P_0^{(1)} + \epsilon^2 P_0^{(2)} + \epsilon \left(P_1^{(1)} \mathrm{e}^{\mathrm{i}\theta} + \mathrm{c.c.} \right)} + \epsilon^2 \left(P_1^{(2)} \mathrm{e}^{\mathrm{i}\theta} + \mathrm{c.c.} \right) \\
& + \epsilon^2 \left(P_2^{(2)} \mathrm{e}^{2\mathrm{i}\theta} + \mathrm{c.c.} \right) + O(\epsilon^3),
\end{aligned}
\tag{3.3}
$$

$$
\begin{aligned}
H = {}& \boxed{\epsilon H_0^{(1)} + \epsilon^2 H_0^{(2)} + \epsilon \left(H_1^{(1)} \mathrm{e}^{\mathrm{i}\theta} + \mathrm{c.c.} \right)} + \epsilon^2 \left(H_1^{(2)} \mathrm{e}^{\mathrm{i}\theta} + \mathrm{c.c.} \right) \\
& + \epsilon^2 \left(H_2^{(2)} \mathrm{e}^{2\mathrm{i}\theta} + \mathrm{c.c.} \right) + O(\epsilon^3),
\end{aligned}
\tag{3.4}
$$

where c.c. stands for complex conjugate of the preceding term in the same braces. The subscript j in all amplitude functions $F_j^{(m)}(z, x_2)$ refers to the harmonic component, and the superscript m refers to the order. The dependence of $F_j^{(m)}$ on the slow coordinate $x_2 = \epsilon^2 x$ corresponds to the anticipated wave attenuation in space. For completeness, all possible terms up to $O(\epsilon^2)$ are included. Only the boxed terms will be needed in the core region for our analysis, however.

First, consider the oscillatory motion in the core. Away from the two oscillatory boundary layers, the first-order waves are well known from the linearized irrotational theory

$$
U_1^{(1)} = \frac{A}{2} \frac{\cosh(kh + z)}{\sinh(kh)}, \quad P_1 = \frac{A}{2} \frac{\cosh(kh + z)}{\sinh(kh)}, \quad W_1^{(1)} = -\mathrm{i} \frac{A}{2} \frac{\sinh(kh + z)}{\sinh(kh)}, \quad H_1 = \frac{A}{2}, \tag{3.5}
$$

where $A = A(x_2)$ is the wave amplitude which is attenuated slowly in x owing to dissipation by turbulence.

Inside the bottom wave boundary layer, the very small laminar viscosity can be ignored. Let the bottom boundary-layer thickness be δ in physical and $\Delta = k\delta$ in normalized forms. It is easy to see that $\Delta = O(\epsilon^2)$ within which the dimensionless eddy viscosity can be approximated by

$$
\epsilon^2 S_T \approx \alpha \epsilon^2 (kh + z), \quad z_b < kh + z < \Delta = k\delta, \tag{3.6}
$$

which is independent of time. The oscillatory longitudinal velocity is (Kajiura 1968),

$$
U_1^{(1)} = \frac{A}{2 \sinh(kh)} (1 - \mathscr{K}(Z)) \mathrm{e}^{\mathrm{i}\theta} + \mathrm{c.c.}, \quad \mathscr{K}(Z) = \frac{K_0 \left(2\sqrt{Z} \mathrm{e}^{-\mathrm{i}\pi/4} \right)}{K_0 \left(2\sqrt{Z_B} \mathrm{e}^{-\mathrm{i}\pi/4} \right)}, \tag{3.7}
$$

where $K_0(Z)$ is the Kelvin function of the zeroth order. Z, Z_B and Z_D are the vertical distances rescaled for the boundary layer as defined by

$$
Z = \frac{kh + z}{\alpha \epsilon^2}, \quad Z_B = \frac{z_b}{\alpha \epsilon^2}, \quad Z_D = \frac{\Delta}{\alpha \epsilon^2}. \tag{3.8}
$$

The oscillatory vertical velocity is

$$
W_1^{(1)} = W_1^{(2)} = 0, \quad W_1^{(3)} = -\alpha \int_{Z_B}^{Z} \frac{\partial U_1^{(1)}}{\partial x} \, \mathrm{d}z. \tag{3.9}
$$

Next, consider the current. At the leading order, the velocity $\epsilon U_0^{(1)}$ is described by the logarithmic law,

$$\epsilon U_0^{(1)} = \frac{U_f/C}{\kappa} \ln\left(\frac{kh+z}{z_b}\right) \equiv \frac{\alpha_0 \epsilon^2}{\kappa^2} \ln\left(\frac{kh+z}{z_b}\right) \quad \text{where } \alpha_0 = \frac{\kappa U_f}{C\epsilon^2} = O(1), \quad (3.10)$$

which vanishes essentially at the apparent bottom $z + kh = z_b$. The factor $\alpha_0 = O(1)$ is the dimensionless form of the friction velocity U_f for the unperturbed current $U_0^{(1)}$.

It should be emphasized that corresponding to the leading-order $O(\epsilon)$ current velocity, the shear rate is

$$\epsilon \frac{\partial U_0^{(1)}}{\partial z} = \frac{\alpha_0 \epsilon^2}{\kappa^2}\left(\frac{1}{kh+z}\right) \equiv \frac{U_f/C}{\kappa}\left(\frac{1}{kh+z}\right), \quad (3.11)$$

which is small ($O(\epsilon^2)$) in the core above the bed, and large ($O(1)$) only inside the oscillatory boundary layer near the bed where $z + kh = O(\epsilon^2)$. Thus, as a consequence of the variable eddy viscosity (if we adopt the model of constant eddy viscosity of order $O(\epsilon^2)$, both the basic current velocity and its shear would be of the same order $O(\epsilon^2)$), the dimensionless current shear in most of the water depth is much smaller than the current velocity ($O(\epsilon^2)$ *vs.* $O(\epsilon)$). Inherent in the CL-II theory, it is the current shear that is crucial to the spanwise instability. Hence, the vortex-forcing mechanism in the weak-current/weak-shear case, i.e. U and U_z are both of order $O(\epsilon^2)$, should still be effective here. Also, the shear rate of the much smaller wave-modified current $\epsilon^2 U_0^{(2)}$, is comparable to that of $\epsilon U_0^{(1)}$; the former has been obtained by Huang & Mei (2003, equation (10.1)) for a hydrodynamically smooth bed,

$$\begin{aligned}
(C_s + \alpha \bar{S})\frac{\partial U_0^{(2)}}{\partial z} &= AA^*\alpha\hat{S}\frac{\sinh(kh+z)}{\sinh(kh)} \pm \frac{\alpha(\alpha-\alpha_0)}{\kappa^2}\left(\frac{-z}{kh}\right) \\
&\quad + \beta AA^*\frac{(z+kh)(2kh+\sinh(2kh))}{8kh\sinh^2(kh)} \\
&\quad + \alpha\frac{AA^*(kh+z)}{2kh\sinh^2(kh)}\int_{Z_B}^{Z_\sigma}\operatorname{Im}(\mathscr{K})\,\mathrm{d}z \\
&\quad - \alpha AA^*\frac{\partial^2 \bar{S}}{\partial z^2}\frac{\sinh(2(kh+z)) - 2(kh+z)}{4\sinh^2(kh)}. \quad (3.12)
\end{aligned}$$

Here, β is the dissipation rate of wave energy, and results in attenuation of wave amplitude $A(x_2)$. The parameter α is the wave-modified dimensionless friction velocity, and differs from the unperturbed value α_0 defined in (3.10).

Inside the bottom wave boundary layer, $U_0^{(2)}$ has been found to be

$$U_0^{(2)}(Z) = \int_{Z_B}^{Z}\frac{\overline{U_1^{(1)}W_1^{(1)}}}{\alpha Z}\,\mathrm{d}z - \left(\pm\frac{\alpha_0 - \alpha}{\kappa^2} + \frac{[\overline{U_1^{(1)}W_1^{(1)}}]_+}{\alpha}\right)\ln\left(\frac{Z}{Z_B}\right), \quad (3.13)$$

where $U_1^{(1)}$ and $W_1^{(1)}$ are the oscillatory boundary-layer velocities given by (3.7) and (3.9). The Reynolds stress everywhere inside the boundary layer is

$$\overline{U_1^{(1)}W_1^{(1)}} = -\frac{\alpha AA^*}{4\sinh^2(kh)}\left[(1 - \mathscr{K}^*)\int_{Z_B}^{Z}\mathrm{i}(1 - \mathscr{K})\,\mathrm{d}z + \text{c.c.}\right]. \quad (3.14)$$

Its value $[\overline{U_1^{(1)}W_1^{(1)}}]_+$ at the upper edge of the bottom boundary layer is taken at the height $z + kh = \Delta$ such that the horizontal orbital velocity is equal to 0.95 times the

inviscid orbital velocity at $z = -kh$. It has been tested in Huang & Mei (2003) that any number greater than 0.95 gives roughly the same numerical result. Details of β and α and numerical computations for $A(x_2)$ and $U_0^{(2)}$ are given in Huang & Mei (2003).

4. Linearized equations for spanwise disturbances to the current
4.1. *Spanwise perturbations*

We now consider time averages with respect to the wave period, and denote by $O(\epsilon\gamma)$ the strength of the time-averaged spanwise-periodic perturbations to the basic current. The order parameter γ is taken to be infinitesimal and independent of ϵ, so that terms of $O(\gamma^2\epsilon^2)$ and smaller can be ignored in the linearized approximation. In order to distinguish the spanwise periodic current from the two-dimensional second-order current $U_0^{(2)}$, the former will be called the *perturbed circulation*.

Through interactions between velocity fields of the steady perturbed circulation of $O(\epsilon\gamma)$ and the primary waves of $O(\epsilon)$, time-harmonic secondary waves of $O(\epsilon^2\gamma)$ will be generated. In turn, interactions between the time-harmonic primary and secondary waves will give rise to a mean Reynolds stress of $O(\epsilon^3\gamma)$, which is steady on the time scale of $1/\omega$ and varies periodically in the transverse (along-crest) direction. This wave-induced mean Reynolds stress corresponds to the *vortex force* in the CL-II theory, and contributes to the slow growth of longitudinal vortices.

As a result of wave attenuation, the slow spatial evolution is described by the slow coordinate $x_2 = \epsilon^2 x$. In order that the unstable growth of perturbed current velocity of order $O(\epsilon\gamma)$ be driven by the mean Reynolds stress of $O(\epsilon^3\gamma)$, the time scale of growth must be of order $O(\epsilon^{-2})$. Therefore we introduce the slow time $t_2 = \epsilon^2 t$ and expand the total longitudinal velocity u as

$$u = U + \epsilon\gamma u_0(z, y, x_2, t_2) + \epsilon^2\gamma \left\{ u_1(z, y, x_2, t_2)\mathrm{e}^{\mathrm{i}\theta} + \text{c.c.} \right\} + O(\epsilon^3, \epsilon^3\gamma, \epsilon\gamma^2), \quad (4.1)$$

where U is the longitudinal velocity of the basic flow given in (3.1), $\epsilon\gamma u_0$ the longitudinal velocity of spanwise perturbations and $\epsilon^2\gamma u_1\mathrm{e}^{\mathrm{i}\theta} + \text{c.c.}$ the longitudinal velocity of secondary waves, where c.c. stands for the complex conjugate of the preceding term. The higher harmonic components of the perturbed waves are smaller than the first harmonic component by a factor of $O(\epsilon)$, hence of $O(\epsilon^3\gamma)$ and not included in (4.1). Similarly, the velocity components v and w can be written as

$$v = \epsilon\gamma v_0(z, y, x_2, t_2) + \epsilon^2\gamma \left\{ v_1(z, y, x_2, t_2)\mathrm{e}^{\mathrm{i}\theta} + \text{c.c.} \right\} + O(\epsilon^3, \epsilon^3\gamma, \epsilon\gamma^2), \quad (4.2a)$$

$$w = W + \epsilon\gamma w_0(z, y, x_2, t_2) + \epsilon^2\gamma \left\{ w_1(z, y, x_2, t_2)\mathrm{e}^{\mathrm{i}\theta} + \text{c.c.} \right\} + O(\epsilon^3, \epsilon^3\gamma, \epsilon\gamma^2). \quad (4.2b)$$

$W = \epsilon(W_1^{(1)}\mathrm{e}^{\mathrm{i}\theta} + \text{c.c.})$ is the vertical velocity of the basic wave field given in (3.2), while $(\epsilon\gamma v_0, \epsilon\gamma w_0)$ are the lateral and vertical mean velocities of perturbed circulation, respectively. In (4.2a) and (4.2b), $\epsilon^2\gamma v_1$ and $\epsilon^2\gamma w_1$ are the lateral and vertical velocity of secondary waves, respectively. Our goal is to derive the governing equations for the perturbed circulation velocities u_0, v_0 and w_0.

In addition, the dynamic pressure p and surface displacement η can also be written as

$$p = P + \epsilon^2\gamma p_0(z, y, x_2, t_2) + \epsilon^2\gamma \left\{ p_1(z, y, x_2, t_2))\mathrm{e}^{\mathrm{i}\theta} + \text{c.c.} \right\} + O(\epsilon^3, \epsilon^3\gamma, \epsilon\gamma^2), \quad (4.3a)$$

$$\eta = H + \epsilon^2\gamma \eta_0(y, x_2, t_2) + \epsilon^2\gamma \left\{ \eta_1(y, x_2, t_2)\mathrm{e}^{\mathrm{i}\theta} + \text{c.c.} \right\} + O(\epsilon^3, \epsilon^3\gamma, \epsilon\gamma^2), \quad (4.3b)$$

where $P = O(\epsilon)$ and $H = O(\epsilon)$ are the dynamic pressure and surface displacement of the basic current given in (3.3) and (3.4). The mean dynamic pressure p_0 and the mean surface displacement η_0 of the perturbed circulation are the results of the interaction

between the basic current of $O(\epsilon)$ and perturbed velocity field of $O(\epsilon\gamma)$, hence are of the order $O(\epsilon^2\gamma)$. Finally, $\epsilon^2\gamma p_1$ and $\epsilon^2\gamma\eta_1$ are the dynamic pressure and surface displacement associated with the secondary waves, in accordance with (4.1) and (4.2).

It should be stressed that the scales of u_0, v_0, w_0 and p_0 are dictated by the magnitude of the shearing rate, rather than the velocity, of the basic current. In the open-channel flow, the current shear is $O(\epsilon^2)$ in the core, although the current velocity is $O(\epsilon)$. It can be shown by using either the Eulerian or the generalized Lagrangian mean formulation and along the lines of Craik (1982b) or Phillips (1998) that the scales of our perturbation circulation are the same as that of the original CL-II theory where both shear and velocity are of order $O(\epsilon^2)$ and weak. This is different from a case studied by Craik (1982b) where both the velocity and the shearing rate of the basic current are of order $O(\epsilon)$. There he finds different scales for the longitudinal vortices: $O(v_0, w_0) = O(\epsilon^{1/2}u_0)$.

4.2. Secondary waves

Since the driving force for unstable growth is of $O(\epsilon^3\gamma)$, we must carry the perturbation analysis to the same order, even though the perturbation velocity itself is of $O(\epsilon\gamma)$. In order to compute the vortex force, we must first solve for the secondary waves of $O(\epsilon^2\gamma)$.

After substituting (4.1)–(4.3b) into the continuity (2.3) and momentum equations (2.4), and collecting the coefficients of $\epsilon^2\gamma e^{i\theta}$, the following linearized equations are obtained for the secondary waves

$$iu_1 + \frac{\partial v_1}{\partial y} + \frac{\partial w_1}{\partial z} = 0, \tag{4.4a}$$

$$-iu_1 + ip_1 = X_1, \tag{4.4b}$$

$$-iv_1 + \frac{\partial p_1}{\partial y} = Y_1, \tag{4.4c}$$

$$-iw_1 + \frac{\partial p_1}{\partial z} = Z_1, \tag{4.4d}$$

where X_1, Y_1, Z_1 represent the nonlinear interactions between the leading-order waves and the perturbed circulation

$$X_1 = -iu_0 U_1^{(1)} - w_0 \frac{\partial U_1^{(1)}}{\partial z} - W_1^{(1)} \frac{\partial u_0}{\partial z}, \tag{4.5a}$$

$$Y_1 = -W_1^{(1)} \frac{\partial v_0}{\partial z}, \tag{4.5b}$$

$$Z_1 = -i u_0 W_1^{(1)} - W_1 \frac{\partial w_0}{\partial z} - w_0 \frac{\partial W_1^{(1)}}{\partial z}. \tag{4.5c}$$

From (4.4) and (4.5), it can be seen that the basic current, $U_0(z) = \epsilon U_0^{(1)} + \epsilon^2 U_0^{(2)} + \cdots$, does not affect the secondary waves directly, but indirectly through the perturbed circulation (u_0, v_0, w_0).

The amplitudes of the oscillatory vorticity components of the secondary waves, $(\xi_1, \vartheta_1, \zeta_1)$, can be obtained from (4.4) by cross-differentiation

$$\xi_1 = \frac{A}{2} \frac{\sinh(kh+z)}{\sinh(kh)} \left(\frac{\partial^2 v_0}{\partial z^2} - \frac{\partial^2 w_0}{\partial z \partial y} - i\frac{\partial u_0}{\partial y} \right) + \frac{A}{2} \frac{\cosh(kh+z)}{\sinh(kh)} \left(\frac{\partial v_0}{\partial z} - \frac{\partial w_0}{\partial y} \right), \tag{4.6a}$$

$$\vartheta_1 = -\frac{A}{2} \frac{\sinh(kh+z)}{\sinh(kh)} \frac{\partial^2 u_0}{\partial z^2}, \tag{4.6b}$$

$$\zeta_1 = -\frac{A}{2} \frac{\sinh(kh+z)}{\sinh(kh)} \left(i\frac{\partial v_0}{\partial z} - \frac{\partial^2 u_0}{\partial z \partial y} - i\frac{\partial w_0}{\partial y} \right) - \frac{A}{2} \frac{\cosh(kh+z)}{\sinh(kh)} \frac{\partial u_0}{\partial y}, \tag{4.6c}$$

where the linear wave solution (3.5) has been used. Note that, in (4.6), the vorticity of the secondary waves is the result of interactions between the primary waves and the perturbed circulation.

Similarly, substituting (4.1)–(4.3b) in the kinematic surface boundary condition (2.16) and the normal stress condition, (2.19) on $z = 0$, and then collecting the coefficients of $\epsilon^2 \gamma e^{i\theta}$, we obtain

$$-i\eta_1 - w_1 = 0, \tag{4.7}$$

$$p_1 - \coth(kh)\eta_1 = 0, \tag{4.8}$$

which are the surface boundary conditions for the secondary waves.

With the governing equations for the secondary waves found, it is now convenient to derive the linearized equations and boundary conditions for the perturbed circulation (u_0, v_0, w_0).

4.3. *Linearized equations for the perturbed circulation*

4.3.1. *Mass conservation*

Substituting (4.1)–(4.3b) into the continuity equation (2.3), collecting the zeroth harmonic terms of $O(\epsilon\gamma)$, we have the following continuity equation for the perturbed circulation

$$\frac{\partial v_0}{\partial y} + \frac{\partial w_0}{\partial z} = 0. \tag{4.9}$$

The longitudinal velocity u_0 does not enter because of its dependence on the slow variable x_2.

4.3.2. *Mean momentum*

Mean longitudinal momentum

Substituting (4.1)–(4.3b) into (2.4), collecting the zeroth harmonic terms of $O(\epsilon^3\gamma)$, we then obtain

$$\frac{\partial u_0}{\partial t_2} + w_0 \left(\frac{\alpha_0}{\kappa} \frac{1}{kh + z} + \frac{\partial U_0^{(2)}}{\partial z} \right) + \left(W_1^{(1)} \right)^* \frac{\partial u_1}{\partial z} + W_1^{(1)} \frac{\partial u_1^*}{\partial z}$$
$$w_1 \frac{\partial \left(U_1^{(1)} \right)^*}{\partial z} + w_1^* \frac{\partial U_1^{(1)}}{\partial z} = \bar{S}_T \frac{\partial^2 u_0}{\partial y^2} + \frac{\partial}{\partial z} \left(\bar{S}_T \frac{\partial u_0}{\partial z} \right), \tag{4.10}$$

where the superscript * represents the complex conjugate. Here,

$$\bar{S}_T = \alpha \bar{S} + C_s = \alpha \left[-z \left(1 + \frac{z}{kh} \right) \right] + C_s \tag{4.11}$$

is the time-independent part of the total viscosity, and dominated by $\bar{S}$ except near the free surface.

The two pairs of complex and conjugate terms on the left-hand side of (4.10) represent interactions between the primary and secondary waves, and can be simplified by using the expression of the vorticity ϑ_1 (4.6b),

$$\frac{\partial u_1}{\partial z} = \vartheta_1 + iw_1 = -\frac{A}{2} \frac{\sinh(kh + z)}{\sinh(kh)} \frac{\partial^2 u_0}{\partial z^2} + iw_1. \tag{4.12}$$

It then follows from (4.12) and the linear wave solutions (3.5) that the sum of the two pairs vanishes. Thus, we finally obtain

$$
\frac{\partial u_0}{\partial t_2} + w_0 \left(\frac{\alpha_0}{\kappa} \frac{1}{kh+z} + \frac{\partial U_0^{(2)}}{\partial z} \right) = \bar{S}_T \frac{\partial^2 u_0}{\partial y^2} + \frac{\partial}{\partial z} \left(\bar{S}_T \frac{\partial u_0}{\partial z} \right).
\tag{4.13}
$$

We note again that the shear rate of $U_0^{(1)}$ and $U_0^{(2)}$ are of comparable importance in the core owing to the logarithmic dependence of $U_0^{(1)}$ on z.

Mean lateral momentum

We now substitute (4.1)–(4.3b) into the lateral momentum equation into (2.11) and collect the zeroth harmonic terms. Expanding $p_0 = p_0^{(2)} + \epsilon p_0^{(3)}$, we obtain at the order $O(\epsilon^2 \gamma)$,

$$
\frac{\partial p_0^{(2)}}{\partial y} + \frac{1}{2} \frac{\partial U_0 u_0}{\partial y} = 0.
\tag{4.14}
$$

At the order $O(\epsilon^3 \gamma)$, we have

$$
\frac{\partial v_0}{\partial t_2} - (W_1^* \xi_1 + \text{c.c.}) + (U_1^* \zeta_1 + \text{c.c.}) + \frac{\partial \Pi_0}{\partial y} = \frac{\partial}{\partial y} \left(2 \bar{S}_T \frac{\partial v_0}{\partial y} \right)
$$
$$
+ \frac{\partial}{\partial z} \left[\bar{S}_T \left(\frac{\partial w_0}{\partial y} + \frac{\partial v_0}{\partial z} \right) \right],
\tag{4.15}
$$

where Π_0 is the pressure head defined by

$$
\Pi_0 = p_0^{(3)} + \tfrac{1}{2} [(U_1^* u_1 + \text{c.c.}) + (W_1^* w_1 + \text{c.c.})].
\tag{4.16}
$$

We shall see shortly that Π_0 can be eliminated from the final vorticity equations, hence its details are immaterial.

The irrotational wave and secondary wave solutions (3.5), (4.6a) and (4.6c) can be used to simplify the second and the third terms on the left-hand side of (4.15). The following equation for the lateral momentum of the perturbed current is obtained

$$
\frac{\partial v_0}{\partial t_2} + \frac{\partial G_0}{\partial y} = \frac{\partial}{\partial y} \left(2 \bar{S}_T \frac{\partial v_0}{\partial y} \right) + \frac{\partial}{\partial z} \left[\bar{S}_T \left(\frac{\partial w_0}{\partial y} + \frac{\partial v_0}{\partial z} \right) \right],
\tag{4.17}
$$

where G_0 is related to the pressure $p_0^{(3)}$ through

$$
G_0 = \Pi_0 + \left(\frac{AA^*}{4} \frac{\sinh(2(kh+z))}{\sinh^2(kh)} \frac{\partial u_0}{\partial z} - \frac{AA^*}{2} \frac{\cosh(2kh+z)}{\sinh^2(kh)} u_0 \right).
\tag{4.18}
$$

Mean vertical momentum

Substituting (4.1)–(4.3b) into the vertical component of (2.11), and collecting the zeroth harmonic terms, we have at the order $O(\epsilon^2 \gamma)$,

$$
\frac{\partial p_0^{(2)}}{\partial z} + \frac{1}{2} \frac{\partial U_0 u_0}{\partial z} = 0.
\tag{4.19}
$$

Together with (4.14), $p_0^{(2)}$ can be solved in principle once the perturbed circulation is found; this is not needed in the sequel. At the order $O(\epsilon^3 \gamma)$, we obtain

$$
\frac{\partial w_0}{\partial t_2} - (U_1 \vartheta^* + \text{c.c.}) + \frac{\partial \Pi_0}{\partial z} = \frac{\partial}{\partial y} \left[\bar{S}_T \left(\frac{\partial w_0}{\partial y} + \frac{\partial v_0}{\partial z} \right) \right] + \frac{\partial}{\partial z} \left(2 \bar{S}_T \frac{\partial w_0}{\partial z} \right).
\tag{4.20}
$$

Making use of (4.6b) to simplify the second term on the right-hand side of (4.20) and recalling the definition of G_0 (4.18), we have

$$\frac{\partial w_0}{\partial t_2} + AA^* u_0 \frac{\sinh(2(kh+z))}{\sinh^2(kh)} + \frac{\partial G_0}{\partial z} = \frac{\partial}{\partial y}\left[\bar{S}_T\left(\frac{\partial w_0}{\partial y} + \frac{\partial v_0}{\partial z}\right)\right] + \frac{\partial}{\partial z}\left(2\bar{S}_T\frac{\partial w_0}{\partial z}\right).$$

$$(4.21)$$

Again, G_0 will be eliminated from the final vorticity equation. The second term on the left-hand side of (4.21) is the vortex force which drives the Langmuir circulation in the CL-II theory (see Craik & Leibovich 1976; Craik 1977).

4.3.3. *Mean vorticity*

Mean longitudinal vorticity

By cross-differentiation of (4.17) and (4.21), the mean longitudinal vorticity $\xi_0 = (w_0)_y - (v_0)_z$ along x is governed by

$$\frac{\partial \xi_0}{\partial t_2} + \frac{\partial u_0}{\partial y}\frac{\partial \bar{U}_s}{\partial z} = \bar{S}_T\left(\frac{\partial^2 \xi_0}{\partial z^2} + \frac{\partial^2 \xi_0}{\partial y^2}\right) - 2\left(\frac{\partial^2 v_0}{\partial y^2} + \frac{\partial^2 v_0}{\partial z^2}\right)\frac{\partial \bar{S}_T}{\partial z}$$
$$- \frac{\partial^2 \bar{S}_T}{\partial z^2}\left(\frac{\partial w_0}{\partial y} + \frac{\partial v_0}{\partial z}\right), \quad (4.22)$$

where $\bar{U}_s$ is the Stokes drift

$$\epsilon^2 \bar{U}_s = \epsilon^2 \frac{AA^*}{2}\frac{\cosh(2(kh+z))}{\sinh^2(kh)}. \quad (4.23)$$

The second term on the left-hand side of (4.22) is the vortex force found by Craik & Leibovich (1976) (see also Craik 1977; Leibovich 1983). Note that the shear $\epsilon^2 \partial \bar{U}_s/\partial z$ associated with Stokes drift is the largest on the free surface and zero at the bottom.

Mean vertical vorticity

For later discussion of the physics, we derive the mean vertical vorticity equation. Because the perturbed circulation is local in x_2, the mean vertical vorticity, ζ_0, is simply

$$\zeta_0 = \epsilon^2 \frac{\partial v_0}{\partial x_2} - \frac{\partial u_0}{\partial y} \approx -\frac{\partial u_0}{\partial y}. \quad (4.24)$$

After taking the y-derivative of (4.13) and making use of (4.24), we have

$$\frac{\partial \zeta_0}{\partial t_2} - \frac{\partial w_0}{\partial y}\left(\frac{\alpha_0}{\kappa}\frac{1}{kh+z} + \frac{\partial U_0^{(2)}}{\partial z}\right) = \bar{S}_T\frac{\partial^2 \zeta_0}{\partial y^2} + \frac{\partial}{\partial z}\left(\bar{S}_T\frac{\partial \zeta_0}{\partial z}\right). \quad (4.25)$$

Thus, the mean vertical vorticity is forced by the interaction between $\partial w_0/\partial y$ (shear due to the upwelling/downwelling motion of the perturbed circulation) and the shearing rate in the basic current, and diffused vertically by turbulence.

The governing equations (4.13) and (4.22) differ from those of Craik and Leibovich only in the details of the basic current and the assumed form of eddy viscosity. In the case of weak shear rate ($O(\epsilon^2)$) and constant eddy viscosity, our linearized field equations are identical to theirs. Note that they do not involve derivatives in x; since variations in the longitudinal direction are slow and only parametric through the local wave amplitude $A(x_2)$. In the next subsection, a new element concerning the surface stress will be derived.

4.4. Linearized free-surface conditions for the perturbed circulation

4.4.1. Kinematic condition

After taking the time average of (2.16) over a wave period, we obtain

$$\epsilon^2 \frac{\partial \overline{\eta}}{\partial t_2} + \epsilon^2 \frac{\partial}{\partial x_2} \overline{\int_0^\eta u \, \mathrm{d}z} + \frac{\partial}{\partial y} \overline{\int_0^\eta v \, \mathrm{d}z} - [\overline{w}]_0 = 0. \tag{4.26}$$

Substituting (4.1)–(4.3b) into (4.26), and collecting terms for the zeroth harmonic components, we obtain the kinematic surface boundary condition

$$w_0 = 0, \quad z = 0, \tag{4.27}$$

which is valid at both $O(\epsilon\gamma)$ and $O(\epsilon^2\gamma)$. Recall from (4.2b) that the mean vertical velocity is $\epsilon\gamma[w_0]_0$ at $z = 0$.

4.4.2. Mean longitudinal shear stress

From (2.23), we obtain for $i = 1$,

$$[\overline{\tau}_{xz}]_0 = -\epsilon^2 \frac{\partial}{\partial t_2} \overline{\int_0^\eta u \, \mathrm{d}z} - \epsilon^2 \frac{\partial}{\partial x_2} \overline{\int_0^\eta u^2 \, \mathrm{d}z} - \frac{\partial}{\partial y} \overline{\int_0^\eta (uv) \, \mathrm{d}z} + [\overline{wu}]_0$$
$$- \epsilon^2 \frac{\partial}{\partial x_2} \overline{\int_0^\eta p \, \mathrm{d}z} + \epsilon^2 \frac{\partial}{\partial x_2} \overline{\int_0^\eta \tau_{xx} \, \mathrm{d}z} + \frac{\partial}{\partial y} \overline{\int_0^\eta \tau_{xy} \, \mathrm{d}z} + \epsilon^2 \frac{\coth(kh)}{2} \frac{\partial \overline{\eta^2}}{\partial x_2}. \tag{4.28}$$

Using the fact that the dimensionless eddy viscosity (2.5) is of $O(\epsilon^2)$, the perturbed circulation velocity $O(\epsilon\gamma)$, and the secondary waves ($\epsilon^2\gamma$), we find, on the left-hand side of (4.28), the mean Reynolds stresses induced by the perturbed circulation to be $O(\epsilon^3\gamma)$ and the oscillatory parts of Reynolds stress associated with the secondary waves to be of $O(\epsilon^4\gamma)$. Substituting (4.1)–(4.3b) into equation (4.28), we find only the third and fourth terms on the right-hand side dominate at $O(\epsilon^3\gamma)$,

$$[\overline{\tau}_{xz}]_0 = -\frac{\partial}{\partial y} \overline{\int_0^\eta (uv) \, \mathrm{d}z} + [\overline{uw}]_0 + O(\epsilon^5\gamma). \tag{4.29}$$

Approximating the right-hand side by using the leading-order terms, we obtain

$$C_s \frac{\partial u_0}{\partial z} = -\left(U_1^{(1)} \big(H_1^{(1)} \big)^* + \big(U_1^{(1)} \big)^* H_1^{(1)} \right) \frac{\partial v_0}{\partial y} + u_1 \big(W_1^{(1)} \big)^* + (u_1)^* W_1^{(1)}$$
$$+ U_1^{(1)} (w_1)^* + \big(U_1^{(1)} \big)^* w_1, \quad z = 0, \tag{4.30}$$

where (4.27) has been used. Details of the derivation are given in Appendix A. Note that on $z = 0$, the steady eddy viscosity vanishes; only the molecular viscosity remains on the left-hand side.

Making use of the linear wave solution (3.5), the right-hand side of (4.30) can be simplified to

$$-\coth(kh)\frac{AA^*}{2} \frac{\partial v_0}{\partial y} + \left(\frac{A^*}{2}[iu_1 + \coth(kh)w_1]_0 + \text{c.c.} \right). \tag{4.31}$$

From the momentum equation (4.4b), and the surface boundary conditions (4.7) and (4.8), we have for the secondary waves

$$i[u_1]_0 = i[p_1]_0 - [X_1]_0, \quad \text{momentum equation,} \tag{4.32a}$$
$$-i\eta_1 - [w_1]_0 = 0, \quad \text{kinematic boundary conditions,} \tag{4.32b}$$
$$[p_1]_0 - \coth(kh)\eta_1 = 0, \quad \text{normal stress boundary conditions,} \tag{4.32c}$$

on $z = 0$. With these, the second term of (4.31) may be written as

$$-\left(\frac{A^*}{2}[X_1]_0 + \frac{A}{2}[(X_1)^*]_0\right) = -\frac{AA^*}{4}\left\{\left(-iu_0\coth(kh) + i\frac{\partial u_0}{\partial z}\right) + \text{c.c.}\right\} \quad (4.33)$$

after further use of the expression (4.5) for X_1. This result clearly vanishes because u_0 is real.

Summarizing the results obtained from (4.30) to (4.33), the surface boundary condition (4.30) can be simplified to

$$\boxed{C_s\frac{\partial u_0}{\partial z} = -\coth(kh)\frac{AA^*}{2}\frac{\partial v_0}{\partial y}.} \quad (4.34)$$

The right-hand side of (4.34) comes from the first term on the right-hand side of (4.30) (or the third term on the right-hand side of (4.28)), and represents the averaged net momentum flux into the unit water column bounded vertically by sides y, $y + dy$, above by the moving free surface and below by $z = 0$. The term is non-zero owing to the interaction between waves and the perturbed circulation.

Equation (4.34) is a key result of this study and differs from the surface condition imposed in the existing CL-II theories. (In Craik & Leibovich (1976) it was assumed without derivation that the perturbed surface stress is zero; a finite wind stress affects only the basic current. In Cox & Leibovich (1993) the perturbed surface stress would be zero if wind were absent.) Note first that the present derivation (in particular, the right-hand side of (4.34)) is independent of the turbulence model chosen. Equation (4.34) would still hold if the eddy viscosity were taken to be constant (i.e. $\alpha = 0$ in (2.8) and ν_T (hence C_s) is replaced by the constant eddy viscosity). This wave-induced surface stress will significantly enhance the internal vortex force which triggers instability via Stokes shear, as will be seen. Note also that this surface-stress condition (4.34) is not directly related to the strength of the basic current U_0. Thus, the surface-stress-driven longitudinal vortices can occur in either a wave-following current, or a wave-opposing current, as long as the current velocity is as strong as the wave orbital velocity in order to maintain the turbulence.

4.4.3. *Mean lateral shear stress*

Similarly, from (4.22) for $i = 2$, we obtain

$$[\bar{\tau}_{yz}]_0 = -\epsilon^2\frac{\partial}{\partial t_2}\overline{\int_0^\eta v\,dz} - \epsilon^2\frac{\partial}{\partial x_2}\overline{\int_0^\eta uv\,dz} - \frac{\partial}{\partial y}\overline{\int_0^\eta (v^2)\,dz} + [\overline{wv}]_0$$
$$- \frac{\partial}{\partial y}\overline{\int_0^\eta p\,dz} + \epsilon^2\frac{\partial}{\partial x_2}\overline{\int_0^\eta \tau_{12}\,dz} + \frac{\partial}{\partial y}\overline{\int_0^\eta \tau_{22}\,dz} + \frac{\coth(kh)}{2}\frac{\partial\overline{\eta^2}}{\partial y}. \quad (4.35)$$

Substituting (4.1)–(4.3b) into the equations (4.35), and collecting the zeroth harmonic components, we find that at $O(\epsilon^2\gamma)$, the surface boundary condition (4.35) is satisfied automatically, but at $O(\epsilon^3\gamma)$, only the fourth, fifth and last terms on the right dominate

$$[\bar{\tau}_{xz}]_0 = [\overline{uw}]_0 - \frac{\partial}{\partial y}\overline{\int_0^\eta p\,dz} + \frac{\coth(kh)}{2}\frac{\partial\overline{\eta^2}}{\partial y} + O(\gamma\epsilon^5), \quad (4.36)$$

which is, to the order $O(\epsilon^3 \gamma)$,

$$C_s \frac{\partial v_0}{\partial z} = \left[W_1^{(1)}(v_1)^* + \left(W_1^{(1)} \right)^* v_1 \right]_0$$

$$- \frac{\partial}{\partial y} \left[\left(P_1^{(1)} \right)^* \eta_1 + P_1^{(1)}(\eta_1)^* + p_1 \left(H_1^{(1)} \right)^* + (p_1)^* H_1^{(1)} \right]_0$$

$$+ \coth(kh) \frac{\partial}{\partial y} \left[\left(H_1^{(1)} \right)^* \eta_1 + H_1^{(1)}(\eta_1)^* \right]_0 + O(\epsilon, \gamma). \qquad (4.37)$$

Details of derivation are similar to those in Appendix A, and are omitted.

Making use of the linear wave solutions (3.5), the right-hand side of (4.37) can be simplified to

$$A^* \left(i[v_1]_0 - \coth(kh) \frac{\partial \eta_1}{\partial y} \right) + \text{c.c.} = A^* \left(i[v_1]_0 - \frac{\partial [p_1]_0}{\partial y} \right) + \text{c.c.}, \qquad (4.38)$$

where (4.32c) has been used. After using the lateral momentum equation (4.4c) and the expression for Y_1, (4.5b), the right-hand side of (4.38) vanishes. Hence, we obtain simply

$$\frac{\partial v_0}{\partial z} = 0, \quad z = 0. \qquad (4.39)$$

Because of this condition and (4.27), the longitudinal vorticity $\xi_0 = \partial w_0/\partial y - \partial v_0 \partial z = 0$ on the mean surface, and can only be generated either from the bottom or in the core by the interaction of the vertical vorticity and the shear in Stokes drift (cf. (4.22)).

4.5. *Bottom boundary conditions for perturbed circulation*

All current velocity components must vanish at the apparent seabed (roughness height),

$$u_0 = v_0 = w_0 = 0, \quad \text{at } z = -kh + z_b. \qquad (4.40)$$

In summary, the velocity fields of the perturbed circulation u_0, v_0, w_0 are governed by (4.13), (4.15) and (4.17), subject to (4.27), (4.34) and (4.39) on $z = 0$ and (4.40) on $z = -kh + z_b$.

5. Eigenvalue problem for spanwise sinusoidal perturbations

We now assume the perturbed circulation motion to be sinusoidal in y.

$$u_0 = \hat{u}_0 \exp(\sigma_2 t_2) \exp(iKy) + \text{c.c.}, \quad v_0 = i \hat{v}_0 \exp(\sigma_2 t_2) \exp(iKy) + \text{c.c.}, \qquad (5.1a)$$

$$w_0 = \hat{w}_0 \exp(\sigma_2 t_2) \exp(iKy) + \text{c.c.}, \quad G_0 = \hat{G}_0 \exp(\sigma_2 t_2) \exp(iKy) + \text{c.c.}, \qquad (5.1b)$$

where the complex parameter σ_2 is to be found as the eigenvalue and the amplitudes $\hat{u}_0, \hat{v}_0, \hat{w}_0$ as eigenfunctions. K is the dimensionless transverse wavenumber and assumed real. Parameter σ_2 is a dimensionless time factor and can be complex. Substituting the normal modes given by (5.1) in the continuity equation (4.9), the momentum equations (4.13), (4.17) and (4.21), as well as the boundary conditions

(4.34), (4.39) and (4.40), we obtain the eigenvalue problem

$$-K\hat{v}_0 + \frac{\partial \hat{w}_0}{\partial z} = 0, \tag{5.2}$$

$$\sigma_2 \hat{u}_0 + \hat{w}_0 \left[\frac{\alpha_0}{kh + z} + \frac{\partial U_0^{(2)}}{\partial z} \right] = -\bar{S}_T K^2 \hat{u}_0 + \frac{\partial}{\partial z} \left(\bar{S}_T \frac{\partial \hat{u}_0}{\partial z} \right), \tag{5.3}$$

$$\sigma_2 \hat{v}_0 + K\hat{G}_0 = -\bar{S}_T K^2 \hat{v}_0 + \frac{\partial}{\partial z} \left(\bar{S}_T \frac{\partial \hat{v}_0}{\partial z} \right) + K\hat{w}_0 \frac{\partial \bar{S}_T}{\partial z}, \tag{5.4}$$

$$\sigma_2 \hat{w}_0 + \hat{u}_0 \frac{\partial U_s}{\partial z} + \frac{\partial \hat{G}_0}{\partial z} = -\bar{S}_T K^2 \hat{w}_0 + \frac{\partial}{\partial z} \left(\bar{S}_T \frac{\partial \hat{w}_0}{\partial z} \right) + K\hat{v}_0 \frac{\partial \bar{S}_T}{\partial z}, \tag{5.5}$$

with boundary conditions

$$C_s \frac{\partial \hat{u}_0}{\partial z} = KAA^* \frac{\coth(kh)}{2} \hat{v}_0, \quad \frac{\partial \hat{v}_0}{\partial z} = 0, \quad \hat{w}_0 = 0, \tag{5.6}$$

on the still-water level $z = 0$, and

$$\hat{w}_0 = 0, \quad \hat{v}_0 = 0, \quad \hat{u}_0 = 0, \tag{5.7}$$

on the bottom $z = -kh + z_b$. Because of the definition of $\hat{v}_0$ in (5.1), all coefficients except σ_2 are real. The eigenvalue σ_2 is, in general, complex and a function of several parameters defining the basic current and waves: $K, \alpha_0, \alpha, kh, z_b$. The current strength U_f/C, the wave steepness ϵ and the depth-to-wavelength ratio kh define the dimensionless ratios $\alpha_0 = \kappa U_f/(C\epsilon^2)$ which may be regarded as the normalized friction factor characterizing the intensity of the basic current, and $\alpha = \alpha(\alpha_0, z_b, kh, \epsilon) = \kappa u_f/(C\epsilon^2)$ which is the normalized wave-modified friction factor. As an eigenfunction is defined only up to a multiplicative factor, numerical results of the eigenfunctions defined in (5.1) will be renormalized so that the initial energy is unity, i.e.,

$$\int_{-kh+z_b}^{0} \langle E_0 \rangle \, \mathrm{d}z = \int_{-kh+z_b}^{0} [\hat{u}_0 \hat{u}_0^* + \hat{v}_0 \hat{v}_0^* + \hat{w}_0 \hat{w}_0^*] \, \mathrm{d}z = 1. \tag{5.8}$$

6. Energy budget of perturbed circulation

6.1. *Equation of mechanical energy*

To facilitate physical discussion we derive below the energy budget of the perturbed circulation. It is convenient to express the Reynolds stresses in terms of the strain rate. The momentum equations (4.13),(4.17) and (4.21), can be rewritten as follows:

$$\frac{\partial u_0}{\partial t_2} + w_0 \left(\frac{\alpha_0}{\kappa} \frac{1}{kh + z} + \frac{\partial U_0^{(2)}}{\partial z} \right) = 2 \left[\frac{\partial}{\partial y}(\bar{S}_T e_{xy}) + \frac{\partial}{\partial z}(\bar{S}_T e_{xz}) \right], \tag{6.1a}$$

$$\frac{\partial v_0}{\partial t_2} + \frac{\partial G_0}{\partial y} = 2 \left[\frac{\partial}{\partial y}(\bar{S}_T e_{yy}) + \frac{\partial}{\partial z}(\bar{S}_T e_{yz}) \right], \tag{6.1b}$$

$$\frac{\partial w_0}{\partial t_2} + AA^* u_0 \frac{\sinh(2(kh + z))}{\sinh^2(kh)} + \frac{\partial G_0}{\partial z} = 2 \left[\frac{\partial}{\partial y}(\bar{S}_T e_{yz}) + \frac{\partial}{\partial z}(\bar{S}_T e_{zz}) \right], \tag{6.1c}$$

where the strain rate e_{ij} has its usual meaning. Let the dimensionless energy density of the perturbed circulation per unit volume be defined by

$$E_0 = \tfrac{1}{2} \left(u_0^2 + v_0^2 + w_0^2 \right). \tag{6.2}$$

Multiplying u_0, v_0, w_0 on both sides of equations (6.1a)–(6.1c), respectively, and summing up the results, we obtain the mechanical energy equation of the perturbed circulation

$$
\frac{\partial E_0}{\partial t_2} = - u_0 w_0 \frac{\partial U_s}{\partial z} - u_0 w_0 \left(\frac{\alpha_0}{\kappa} \frac{1}{kh+z} + \frac{\partial U_0^{(2)}}{\partial z} \right) - 2\bar{S}_T \left(2e_{xy}^2 + 2e_{xz}^2 + e_{yy}^2 + 2e_{yz}^2 + e_{zz}^2 \right)
$$
$$
+ \frac{\partial}{\partial y} \left(2\bar{S}_T \left(e_{xy} u_0 + e_{yy} v_0 + e_{yz} w_0 \right) - G_0 v_0 \right)
$$
$$
+ \frac{\partial}{\partial z} \left(2\bar{S}_T \left(e_{xz} u_0 + e_{yz} v_0 + e_{zz} w_0 \right) - G_0 w_0 \right). \tag{6.3}
$$

We now restrict ourselves to spanwise periodic perturbations and consider a control volume extending laterally in y over a transverse wavelength $2\pi/K$, longitudinally over a unit length, and vertically from the apparent bottom to the mean surface. Integrating (5.1) over this control volume we obtain

$$
\frac{\partial}{\partial t_2} \int_{-kh+z_b}^0 \langle E_0 \rangle \, \mathrm{d}z = - \int_{-kh+z_b}^0 \langle u_0 w_0 \rangle \frac{\partial U_s}{\partial z} \, \mathrm{d}z - \int_{-kh+z_b}^0 \frac{\alpha_0}{\kappa} \frac{\langle u_0 w_0 \rangle}{kh+z} \, \mathrm{d}z
$$
$$
- \int_{-kh+z_b}^0 \langle u_0 w_0 \rangle \frac{\partial U_0^{(2)}}{\partial z} \, \mathrm{d}z + \left[2C_s \langle e_{xz} u_0 \rangle \right]_0
$$
$$
- 2 \int_{-kh+z_b}^0 \bar{S}_T \langle 2e_{xy}^2 + 2e_{xz}^2 + e_{yy}^2 + 2e_{yz}^2 + e_{zz}^2 \rangle \, \mathrm{d}z, \tag{6.4}
$$

where $\langle F \rangle$ signifies area integral of F over the horizontal extent of $2\pi/K \times 1$. Spanwise periodicity and the bottom and surface boundary conditions, (4.40), (4.34) and (4.39) have been used.

The free-surface term (fourth term on the right-hand side) can be written as

$$
C_s \left\langle \frac{\partial u_0}{\partial z} u_0 \right\rangle_0 = - \frac{AA^* \coth(kh)}{2} \left\langle u_0 \frac{\partial v_0}{\partial y} \right\rangle_0, \tag{6.5}
$$

where the surface conditions (4.34) and (4.27) have been used. Note also that in (6.4), G_0 disappears by periodicity and the boundary conditions on $z = -kh + z_b$ and $z = 0$. While all terms in (6.4) are interdependent, being parts of the solution to the same problem, each plays its own physical role. In the order of their appearance, the first three terms on the right-hand side are, respectively, the rate of energy production by Reynolds' stress against the velocity shears in (i) the Stokes drift, (ii) the unperturbed ambient current, and (iii) the wave-induced current correction. The fourth term represents the rate of work done by the mean surface stress with the horizontal velocity. The last term is the rate of energy dissipation by turbulence.

Let the eigenvalue σ_2 be complex, and let $\sigma = \epsilon^2 \sigma_2 = \sigma_r + \mathrm{i}\sigma_i$. The real part σ_r is the growth rate of the perturbed circulation on the unstretched time t scaled by $1/\omega$. Since the energy growth rate on the unstretched time t is $\sigma_E = 2\sigma_r = 2\mathrm{Re}(\sigma)$, the energy budget (6.4) can be written as

$$
\sigma_r = \sigma_{st} + \sigma_{u_1} + \sigma_{u_2} + \sigma_{sw} - \sigma_\varepsilon,
$$

where each term is the counterpart of the successive terms in (6.4),

$$\sigma_{st} = \frac{\epsilon^2}{2} \int_{-kh+z_b}^{0} (-\hat{u}_0 \hat{w}_0^* + \text{c.c.}) \frac{\partial U_s}{\partial z} \, \mathrm{d}z, \tag{6.6a}$$

$$\sigma_{u_1} = \frac{\epsilon^2}{2} \int_{-kh+z_b}^{0} \frac{\alpha_0}{\kappa^2} \frac{\langle -u_0 w_0 \rangle}{kh+z} \, \mathrm{d}z \equiv \frac{U_f/C}{2\kappa} \int_{-kh+z_b}^{0} \frac{(-\hat{u}_0 \hat{w}_0^* + \text{c.c.})}{kh+z} \, \mathrm{d}z, \tag{6.6b}$$

$$\sigma_{u_2} = \frac{\epsilon^2}{2} \int_{-kh+z_b}^{0} (-\hat{u}_0 \hat{w}_0^* + \text{c.c.}) \frac{\partial U_0^{(2)}}{\partial z} \, \mathrm{d}z, \tag{6.6c}$$

$$\sigma_{sw} = \frac{\epsilon^2}{2} K [\hat{v}_0 \hat{u}_0^* + \text{c.c.}]_0 A A^* \frac{\coth(kh)}{2}, \tag{6.6d}$$

$$\sigma_{\varepsilon} = \frac{\epsilon^2}{2} \int_{-kh+z_b}^{0} 2(C_s + \alpha \bar{S}) \phi(z) \, \mathrm{d}z \equiv \int_{-kh+z_b}^{0} \left(\frac{k^2 \nu}{\omega} + \kappa \frac{u_f}{C} \bar{S} \right) \phi(z) \, \mathrm{d}z, \tag{6.6e}$$

where ϕ is the amplitude of the dissipation function,

$$\phi(z) = K^2 |\hat{u}_0|^2 + \left| \frac{\partial \hat{u}_0}{\partial z} \right|^2 + 2K^2 |\hat{v}_0|^2 + 2 \left| \frac{\partial \hat{w}_0}{\partial z} \right|^2 + \left| \frac{\partial \hat{v}_0}{\partial z} + \mathrm{i} K \hat{w}_0 \right|^2.$$

It can be seen that the Reynolds stress $(-\hat{u}_0 \hat{w}_0^* + \text{c.c.})$ induced by the spanwise perturbation affects the energy input rates σ_{st}, σ_{u_1} and σ_{u_2} and σ_{sw} under given wave and current conditions. The magnitudes of these contributions will be compared later from numerical solutions with a view to understanding the relative importance of Stokes drift and the surface stress. Now let us first examine the physical role of the mean surface stress on instability.

7. Physics of instability

In CL-II theory (Craik 1977; Leibovich 1983; etc.), any spanwise perturbation of u_0 gives rise to new vertical vorticity $\zeta_0 = -\partial u_0/\partial y$. Through the longitudinal vortex force (the second term on the left-hand side of (4.22)), the longitudinal vorticity is increased by the Stokes drift. Then, through the vertical vortex force term on the left-hand side of (4.25), shear in the primary current helps produce new vertical vorticity. These two 'vortex forces' reinforce each other and lead to instability. In an inviscid flow, the necessary condition for instability (1.1) is independent of the spanwise perturbations.

In our problem, the internal driving forces in CL-II theory are still present. Their contributions to energy production are represented by σ_{st} (Stokes drift) and $\sigma_{u_1} + \sigma_{u_2}$ (basic current) in (6.6). Because w_0 is zero on the bottom and the mean sea surface, these driving forces are effective only in the core region where the shearing rate is, however, not the highest. We now show that σ_{sw} supplies an additional source from the top surface to augment the CL-II mechanism.

On the mean surface, the longitudinal stress condition (4.34) can be written as

$$C_s \frac{\partial u_0}{\partial z} = A A^* \frac{\coth(kh)}{2} \frac{\partial w_0}{\partial z}, \tag{7.1}$$

after using the continuity equation for the perturbed circulation, (4.9). Taking the y-derivative of (7.1), we obtain

$$-C_s \frac{\partial \zeta_0}{\partial z} = A A^* \frac{\coth(kh)}{2} \frac{\partial}{\partial z} \left(\frac{\partial w_0}{\partial y} \right), \quad z = 0. \tag{7.2}$$
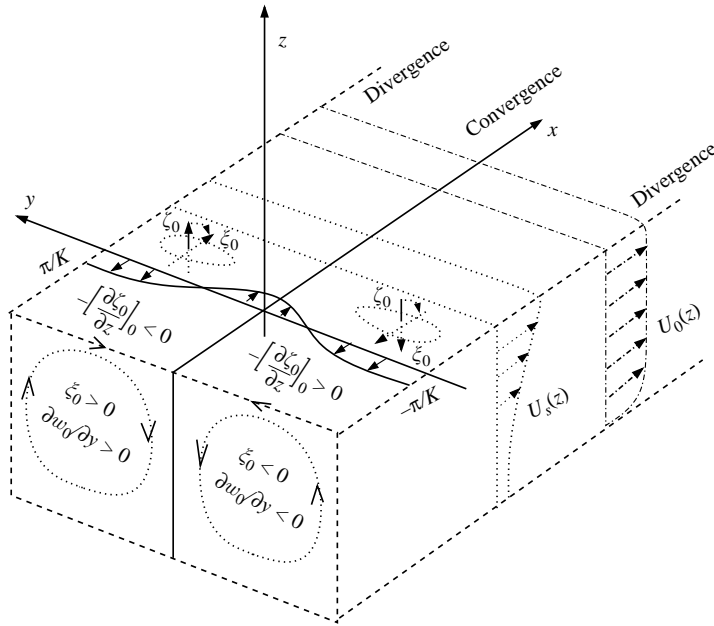
FIGURE 1. Effects of the surface stress.

Since near $z = 0$, C_s is the dominant part of the total effective viscosity S_T, the preceding condition states that there is an influx (or outflux) of the vertical vorticity component ζ_0 from the mean surface downward. This boundary flux is transported vertically to the core according to the convective-diffusion equation (4.25). We now examine the sign of this vorticity flux.

Referring to figure 1, if there is spanwise periodic divergence/convergence near the free surface toward lines parallel to the x-axis, there must be upwelling and downwelling in a cross-sectional plane, as sketched. On the side of $\pi/K > y > 0$, $\partial w_0/\partial y > 0$ in the core, but vanishes on the free surface where $w_0 = 0$ everywhere. Hence, its vertical gradient is negative near the free surface and $-\partial\zeta_0/\partial z < 0$, meaning that there is a downward flux of positive vertical vorticity from the upper boundary. This influx is then transported downward according to (4.25) to increase the vertical vorticity in the core. Now the CL-II mechanism takes over, i.e. the increment of $\zeta_0 = -\partial u_0/\partial y$ forces further increase of the longitudinal vorticity ξ_0 by vortex force associated with the Stokes drift, according to (4.22). This increment then augments the vortex force in (4.22) and increases the longitudinal vorticity via the CL-II mechanism. On the side $-\pi/K < y < 0$, all signs are reversed; a counter-rotating vortex in the x-direction also grows.

Leaving the details of numerical computations to Appendix B, we now discuss the numerical results. All the examples given below are obtained by setting $AA^* = 1$, since the linear stability analysis is local in x and does not involve longitudinal gradients. The growth rate of the perturbed circulation will be presented for the unstretched time t. The numerical values of the typical input parameters are given in Appendix C.

8. Longitudinal vortices in a wave-following current

Following the procedure of Huang & Mei (2003), we first calculate the basic current $\epsilon U_0^{(1)}$ and the second-order modification by waves $\epsilon^2 U_0^{(2)}$. Typical shear profiles of
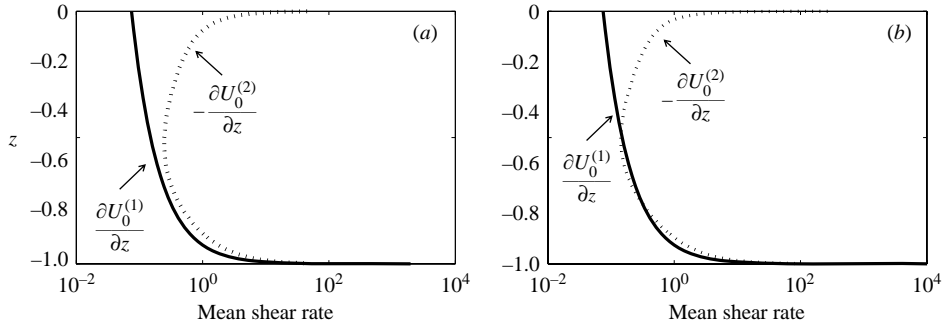
FIGURE 2. Typical shear rates in a wave-following current. Solid line: the unperturbed current; dashed line: the perturbed current. Note the difference in signs. Input parameters are $kh = 1$, $U_f/C = 0.003$, $\epsilon = 0.1$. (a) $h = 0.5\,\text{m}$; (b) $h = 3\,\text{m}$.
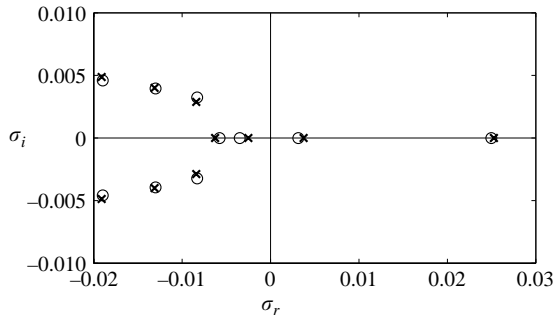

FIGURE 3. The first 10 eigenvalues for wave-following current: $kh = 1$, $U_f/C = 0.002$, $\epsilon = 0.1$ and $K = 3$. $\bigcirc$, $h = 0.5\,\text{m}$; $\times$, $h = 3\,\text{m}$.

a wave-following current are shown in figure 2 for $h = 0.5\,\text{m}$ (laboratory flume) and $h = 3\,\text{m}$ (shallow lake), respectively. It can be seen that $\mathrm{d}U_0^{(2)}/\mathrm{d}z \gg \mathrm{d}U_0^{(1)}/\mathrm{d}z$ above the mid depth so that $\epsilon^2 \mathrm{d}U_0^{(2)}/\mathrm{d}z \sim \epsilon \mathrm{d}U_0^{(1)}/\mathrm{d}z$, and the shear rates in both the basic current and in the wave-induced current can be comparable. Note also that $\mathrm{d}U_0^{(1)}/\mathrm{d}z$ in the basic current is positive throughout the water depth especially near the bed, as is the shear in Stokes drift, hence destabilizing according to criterion (1.1). However, shear in the second-order wave-induced current $\mathrm{d}U_0^{(2)}/\mathrm{d}z$ in figure 2 is negative, hence stabilizing instead.

8.1. *Existence of unstable modes*

The real and imaginary parts of the first 10 eigenvalues are plotted in figure 3 for two depths: $h = 0.5, 3\,\text{m}$. In both cases, only two unstable modes are found. For $h = 0.5\,\text{m}$, the first mode has a growth rate $\sigma_r = 0.0248$ and the second $\sigma_r = 0.0031$. For $h = 3\,\text{m}$, the first mode has a growth rate $\sigma_r = 0.0254$ and the second $\sigma_r = 0.0034$. For these unstable modes $\sigma_i = 0$, hence the principle of exchange of instabilities holds. All stable modes are complex-conjugate pairs and the eigenvalues are symmetric about the real axis, since all the coefficients of the governing conditions are real.

Let the streamfunction ψ be defined such that $v_0 = -\partial \psi/\partial z$, $w_0 = \partial \psi/\partial y$. The typical eigenfunctions and the streamline pattern of the first mode are given in figure 4. The eigenfunctions have been normalized so that $\hat{u}_0$ is real and positive on the mean water surface. For this mode, the vertical vorticity (or longitudinal velocity
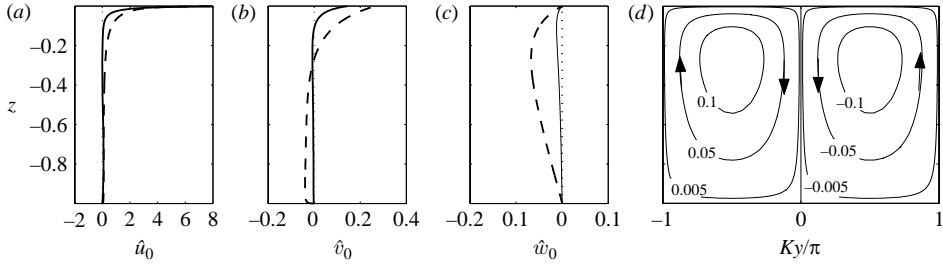
FIGURE 4. Typical profiles of the eigenfunctions and the cell pattern for the first eigen mode. Inputs are: $kh = 1$, $U_f/C = 0.002$, $K = 3$. The mean depth is $h = 3$ m. (a–c) The velocity components of the eigenfunction. Solid curves: $\epsilon = 0.1$. Dashed curves: $\epsilon = 0.05$. (d) The contours of the transverse streamfunction for $\epsilon = 0.05$, where the numbers indicate the values of the streamfunction.
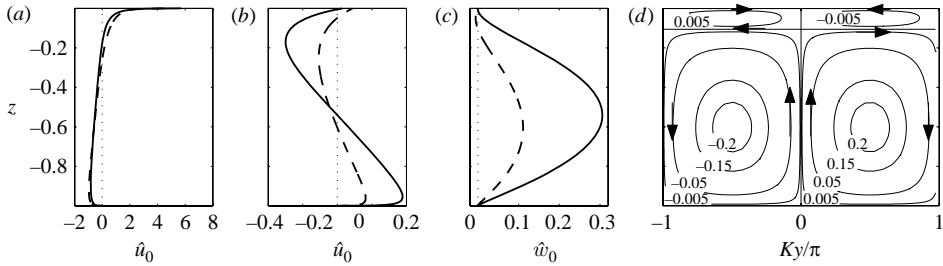

FIGURE 5. As figure 4, but for the second eigenmode.

$\hat{u}_0$) does not change sign in the entire water depth. The longitudinal axes of the vortices are high near the free surface, as shown in figure 4. The strength of the longitudinal vortices decreases with increasing wave slope, as indicated by the profile of the vertical velocity. The dimensionless diffusivity $\alpha = \kappa u_f/C\epsilon^2$ in the vorticity equation (4.25), which represents the ratio of vorticity diffusion by turbulence to production by waves, decreases with increasing wave slope ϵ. Physically, for stronger waves, the vertical vorticity produced by waves is less diffused from the surface to the core. A large gradient of the vertical vorticity is therefore present near the surface. Thus, for the first mode, stronger waves induce less mixing with the sea bottom.

The typical eigenfunctions and the cell pattern of the second mode are given in figure 5. There are two pairs of cells. Near the free surface, the cells are smaller and circulate in the same directions as the cells in the first mode. They are directly influenced by the mean surface stress. Near the seabed, the cells circulate in the opposite directions and interact more strongly with the seabed.

8.2. *Effects of wave slope ϵ and spanwise wavenumber K*

The growth rates σ_r of the first and the second eigenmodes are shown in figures 6 and 7 for the following inputs: $kh = 1$, $U_f/C = 0.003$, $\epsilon \in [0.005, 0.16]$, $K \in [0.2, 8]$.

8.2.1. *First unstable mode*

It can be seen from figure 6 that all perturbations are stable if the wave steepness is below $\epsilon < 0.02$. Above this threshold, the growth rate σ_r increases monotonically with increasing wave slope ϵ for any transverse wavenumber K. For gentle waves with slope $0.02 < \epsilon < 0.04$, the growth rate has a maximum about $K = 1 \sim 3$. For steeper waves with $\epsilon > 0.04$, the growth rate increase monotonically with increasing K.
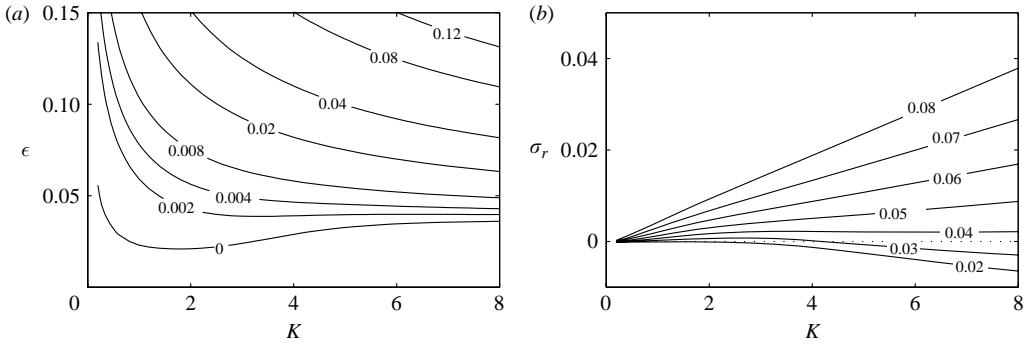
FIGURE 6. Growth rate $\sigma_r(\epsilon, K)$ for the first unstable mode for $kh = 1.0$ and $U_f/C = 0.003$. (*a*) The number on each line represents the value of the growth rate. (*b*) The number on each line represents the wave slope ϵ.

ϵ	σ_{st}	σ_{u_1}	σ_{u_2}	σ_{sw}	σ_{ε}	σ_r
3×10^{-2}	8.28×10^{-5}	1.68×10^{-3}	-2.45×10^{-5}	2.41×10^{-3}	3.43×10^{-3}	7.06×10^{-4}
5×10^{-2}	1.65×10^{-4}	6.70×10^{-4}	-4.49×10^{-5}	2.54×10^{-2}	2.20×10^{-2}	4.17×10^{-3}
7×10^{-2}	1.14×10^{-4}	1.28×10^{-4}	-3.87×10^{-5}	6.28×10^{-2}	5.27×10^{-2}	1.01×10^{-2}

TABLE 1. Effect of wave slope on the energy budget of the first eigenmode in a wave-following current for $kh = 1$, $U_f/C = 0.003$.

To understand how the wave slope affects instability through the basic current $U_0^{(1)}$, the Stokes drift U_s, the wave-induced current $U_0^{(2)}$ and the surface stress, we list the various contributions to the energy growth rate σ_r in table 1 for $h = 3$ m, $K = 3$ and $\epsilon = 0.03, 0.05, 0.07$. Not surprisingly, the growth rate σ_r increases with the wave slope ϵ. Thus, the first unstable mode will reach the nonlinear stage very quickly for large wave slope. The most important stabilizer is dissipation, represented by σ_{ε}. From (6.6*e*), the dissipation rate is dominated by the shear rate $\partial u_0/\partial z$ near the water surface, which vanished as the wave slope tends to zero (cf. (4.34)). Therefore, for a given current strength, σ_{ε} decreases with decreasing wave slope. For all wave slopes, σ_{u_1} and σ_{st} are positive, thus they are destabilizing. However, σ_{u_2} is negative for all wave slopes, indicating that the wave-modified secondary current is a weak stabilizing force. The most important destabilizer is the mean surface stress, represented by σ_{sw}, which increases with wave slope. For small wave slope, the destabilizing contribution of $U_0^{(1)}$ can be comparable to that of σ_{sw}.

From figure 6 it can be seen for steep waves that the growth rate of the first eigenmode is almost linear in K, hence smaller cells grow faster.

8.2.2. *Second unstable mode*

As can be seen in figure 7, the second mode is unstable only when the wave slope exceeds the threshold $\epsilon > 0.05$ and the wavenumber K lies within a finite range. In other words, the sizes of the longitudinal cells are limited to a finite range within which there is a preferred transverse wavenumber K for any wave slope ϵ. As shown in figure 7(*a*), the preferred transverse wavenumber increases slightly with increasing wave slope, indicating that the size of the most unstable cell decreases with steeper waves.
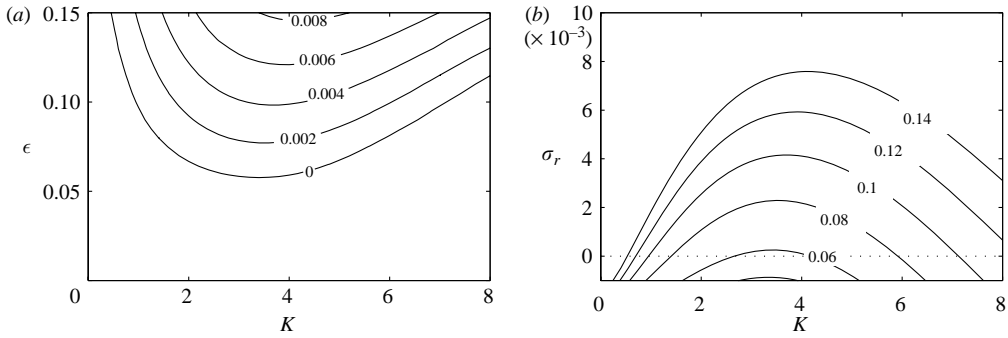
FIGURE 7. Growth rate $\sigma(\epsilon, K)$ for the second unstable mode for $kh = 1.0$ and $U_f/C = 0.003$. (*a*) The number on each line represents the growth rate. (*b*) The number on each line represents the wave slope.

ϵ	σ_{st}	σ_{u_1}	σ_{u_2}	σ_{sw}	σ_ε	σ_r
6×10^{-2}	1.22×10^{-4}	2.21×10^{-3}	-1.02×10^{-4}	5.99×10^{-3}	8.02×10^{-3}	1.80×10^{-4}
8×10^{-2}	3.68×10^{-4}	3.36×10^{-3}	-2.58×10^{-4}	8.85×10^{-3}	1.01×10^{-2}	2.15×10^{-3}
10×10^{-2}	8.29×10^{-4}	4.38×10^{-3}	-5.13×10^{-4}	1.03×10^{-2}	1.11×10^{-2}	3.90×10^{-3}

TABLE 2. Effect of wave slope on the energy budget of the second eigenmode in a wave-following current.

The computed values of σ_{st}, σ_{u_1}, σ_{u_2}, $\sigma_{u_{sw}}$ and σ_ε are given in table 2 for $U_f/C = 0.003$, $kh = 1$, $K = 3$ and $\epsilon = 0.06, 0.08, 0.10$. The growth rate σ_r again increases with the wave slope. Also the major stabilizer is the dissipation term σ_ε, which is dominated by the shear rates in the perturbed current near the two boundaries, as shown in figure 5. Now $\sigma_{u_2} < 0$, thus the wave-modified secondary current $U_0^{(2)}$ is another stabilizer, although much smaller than σ_ε. As shown in the velocity profiles in figure 5, the vertical shearing rates in w_0 increases with increasing wave slope, but the shear rate in u_0 changes little. As a result, σ_ε changes only slightly with increasing wave slope. In comparison with the contributions from the surface stress (σ_{sw}), the shearing rates in the Stokes drift (σ_{st}) and in the primary current (σ_{u_1}) are comparably important to the total growth rate (σ_r). Thus, for the second unstable mode the surface stress and the internal shears are equally effective. With larger waves, values of σ_{u_1} and σ_{st} increase, as is typical of the CL-II mechanism. As in the first unstable mode, the contribution of σ_{sw} is reduced as the wave slope becomes smaller. Note that σ_{st} is in general smaller than σ_{u_1} and σ_{sw}.

8.3. *Effects of wavelength*

The growth rates of the first and the second eigenmodes are plotted in figures 8 and 9, for kh ranging from 0.2 to 8, for fixed $h = 3$ m. As a reference, $kh = 0.2$ corresponds to wavelength 94 m ($k = 0.067 \text{ m}^{-1}$) and $kh = 8$ to wavelength 2.35 m ($k = 2.67 \text{ m}^{-1}$) in water of depth $h = 3$ m.

For a given current strength and wave slope, the growth rate of the first unstable mode increases almost linearly with K for given kh, and decreases with increasing kh when waves are not too short ($kh < 2$). For very short waves (or very deep water) instability is of course not affected by the water depth.
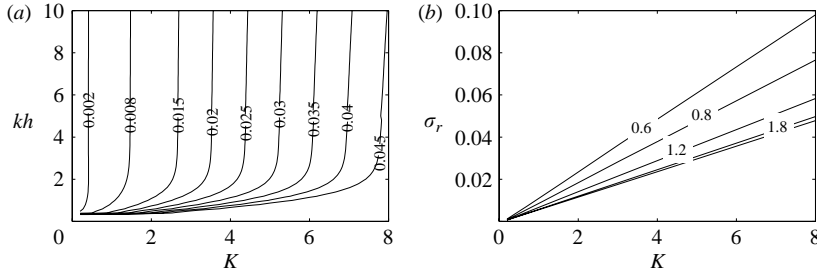
FIGURE 8. Effect of kh on the growth rate $\sigma_r(K; kh)$ of the first mode for $U_f/C = 0.003$ and $\epsilon = 0.1$. (*a*) The number on each line represents the value of the growth rate σ_r. (*b*) The number on each line represents the dimensionless depth kh.
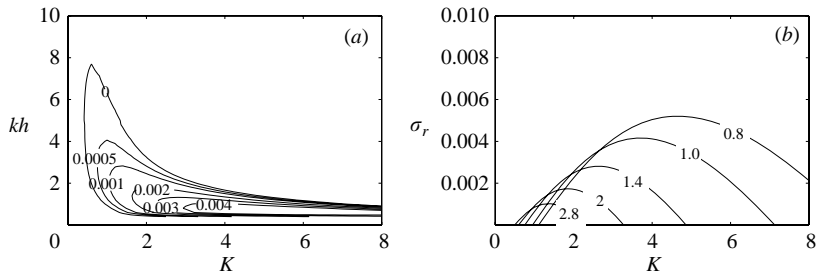

FIGURE 9. As figure 8, but for the second mode.

kh	σ_{st}	σ_{u_1}	σ_{u_2}	σ_{sw}	σ_ε	σ_r
0.5	1.11×10^{-3}	6.55×10^{-3}	-3.57×10^{-3}	5.55×10^{-3}	6.83×10^{-3}	2.80×10^{-3}
1.0	8.29×10^{-4}	4.38×10^{-3}	-5.13×10^{-4}	1.03×10^{-2}	1.11×10^{-2}	3.90×10^{-3}
1.5	6.76×10^{-4}	3.75×10^{-3}	-5.06×10^{-6}	4.82×10^{-3}	6.88×10^{-3}	2.35×10^{-3}
2.0	5.21×10^{-4}	2.85×10^{-3}	2.27×10^{-4}	2.41×10^{-3}	5.43×10^{-3}	5.61×10^{-4}

TABLE 3. Effect of kh on the energy budget of the second eigenmode.

Now the second unstable mode. For a given transverse wavenumber K, the growth rate first increases and then decreases with increasing kh. Thus, the growth rate is greater in shallower water. For a given relative depth (kh), there is a preferred cell size (K) corresponding to the fastest growth. For a fixed wave steepness there is a maximum depth beyond which the second mode is no longer unstable. Note that the maximum growth rate is larger for smaller kh, but the size of the fastest growing cell increases with kh.

The energy budget of the second mode is given in table 3 for $K = 3$ and $kh = 0.5$ to 2.0. The depth range $kh > 2.5$ is of no interest since $\sigma_r < 0$. For small kh, $\sigma_{u_1} \sim \sigma_{sw} > \sigma_{st}$; thus both the basic-current shear and the surface stress are equally important. Note also that for $kh < 1.5$, σ_{u_2} is negative and comparable to σ_{u_1}, hence shear in the secondary current is stabilizing. For large kh, σ_{u_1} and σ_{sw} become comparable; unstable growth is driven by both the surface stress and the internal shear. The dimensionless shear rate reduces with the increase in kh, leading to a reduction in σ_{u_1}. Also, σ_{sw} does not change monotonically with kh. In this example, there is a maximum between $kh = 1$ and $kh = 1.5$. The Reynolds stress due to perturbed
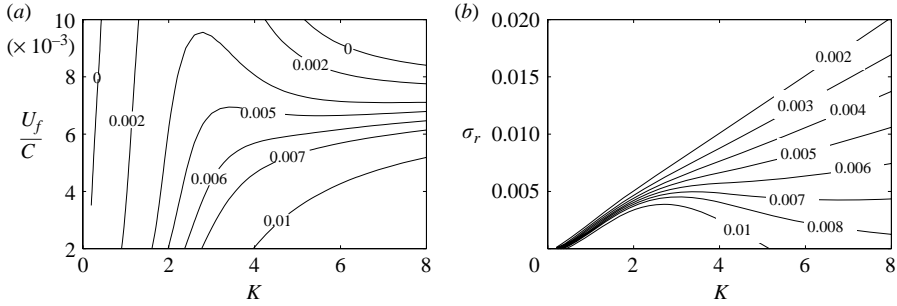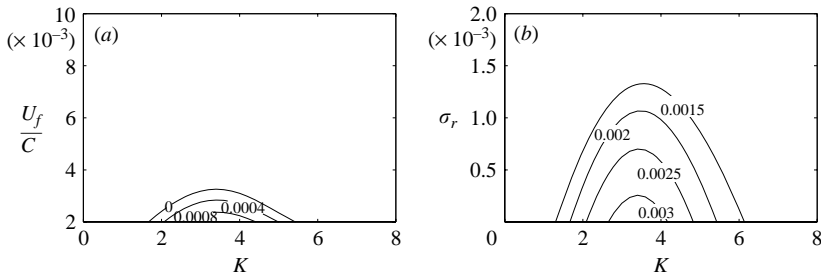
FIGURE 10. Effect of U_f/C on the growth rate $\sigma_r(K; U_f/C)$ of the first mode for $kh = 1.0$ and $\epsilon = 0.06$. (*a*) The number on each line indicates the growth rate σ_r. (*b*) The number on each line indicates the current strength U_f/C.

FIGURE 11. Effect of U_f/C on the growth rate $\sigma_r(K; U_f/C)$ of the second mode for $kh = 1.0$ and $\epsilon = 0.06$. (*a*) The number on each line indicates the growth rate σ_r. (*b*) The number on each line indicates the current strength U_f/C.

current, $\langle -u_0 w_0 \rangle$, may be negative in a region near the surface, as can be inferred from the shape of eigenfunctions in figure 5. Near the surface, the shear rate in the wave-modified secondary current $U_0^{(2)}$ is relatively large, thus a small positive σ_{u_2} is possible, as shown in table 3 for $kh > 1.5$, which implies that the wave-modified secondary current may, to some extent, destabilize the basic current. For all kh, the contribution from the Stokes-drift shear σ_{st} is comparable to the total growth rate.

8.4. *Effect of current strength*

The change of the growth rate with the current strength U_f/C is illustrated in figure 10 for the first and figure 11 for the second unstable mode. The growth rate of the first mode increases with decreasing U_f/C for all transverse wavenumbers. For a sufficiently strong current with $U_f/C > 0.007$, there is a preferred transverse wavenumber corresponding to the largest growth rate. Beyond a certain threshold (outside the range of validity here), disturbances of all K are stable. This is to be expected since in an increasingly strong current, the effects of waves of fixed intensity diminish. For very small U_f/C, the growth rate is almost linear in K, similar to the case of very large wave slope. Thus, weak current and large wave slope have the same effect on $\alpha = \kappa \epsilon^{-2} U_f/C$, which represents the ratio of the vorticity diffusion by turbulence and production by waves.

The energy budget of the first eigenmode is given in table 4 for various U_f/C. Contribution by the basic current represented by σ_{u_1} is much smaller than that of the surface stress σ_{sw} for small U_f/C, but comparable to σ_{sw} for large U_f/C. In a weak

U_f/C	σ_{st}	σ_{u_1}	σ_{u_2}	σ_{sw}	σ_ε	σ_r
2.00×10^{-3}	7.13×10^{-5}	6.78×10^{-5}	-3.03×10^{-5}	4.41×10^{-2}	3.65×10^{-2}	7.58×10^{-3}
4.00×10^{-3}	2.15×10^{-4}	7.58×10^{-4}	-5.44×10^{-5}	3.98×10^{-2}	3.44×10^{-2}	6.18×10^{-3}
6.00×10^{-3}	3.16×10^{-4}	2.34×10^{-3}	-8.04×10^{-5}	2.94×10^{-2}	2.66×10^{-2}	5.26×10^{-3}
9.00×10^{-3}	3.46×10^{-4}	4.87×10^{-3}	-1.10×10^{-4}	1.72×10^{-2}	1.81×10^{-2}	4.11×10^{-3}

TABLE 4. Effect of U_f/C on the energy budget of the first eigenmode for $kh = 1.0$ and $\epsilon = 0.06$.

U_f/C	σ_{st}	σ_{u_1}	σ_{u_2}	σ_{sw}	σ_ε	σ_r
1.50×10^{-3}	2.31×10^{-4}	1.80×10^{-3}	-1.44×10^{-4}	4.22×10^{-3}	4.85×10^{-3}	1.25×10^{-3}
2.00×10^{-3}	1.79×10^{-4}	1.99×10^{-3}	-1.26×10^{-4}	5.12×10^{-3}	6.16×10^{-3}	9.90×10^{-4}
2.50×10^{-3}	1.45×10^{-4}	2.12×10^{-3}	-1.11×10^{-4}	5.69×10^{-3}	7.20×10^{-3}	6.25×10^{-4}
3.00×10^{-3}	1.22×10^{-4}	2.21×10^{-3}	-1.02×10^{-4}	5.99×10^{-3}	8.02×10^{-3}	1.80×10^{-4}

TABLE 5. Effect of U_f/C on the energy budget of the second eigenmode for $kh = 1.0$ and $\epsilon = 0.06$.

current, vorticity cannot be easily diffused from the mean free surface to the core region where Stokes drift is important. The surface stress is the dominant destabilizer for the first mode. In a strong current, vorticity can be more easily diffused down to the core region where Stokes drift is important. Both the surface stress and the internal shear are effective.

For the second mode, there is always a preferred transverse wavenumber (about $K = 3.5$ in the example of figure 11). The growth rate decreases with increasing current strength. Beyond the critical current strength (about $U_f/C = 0.0034$ for $\epsilon = 0.06, kh = 1$) the second mode is stable for all K. This critical value is much smaller than that of the first eigenmode.

The energy budget of the second mode is given in table 5 for various U_f/C. Again, both σ_ε and σ_{sw} are not sensitive to the change of current strength as in the first unstable mode. For the wave slope considered here, σ_{u_1} is comparable to σ_{sw} for all values of U_f/C, so the second eigenmode is equally driven by both the surface stress and the internal shear.

In summary, in a weak current, both the first and the second eigenmode are possible, but in a strong current, only the first eigenmode is possible. The stronger (weaker) current affects the growth rate in the same way as the steeper (milder) wave slope. To have some idea of the physical magnitudes, we take for illustration: wavelength $= 40$ m, wave amplitude $= 0.39$ m, current friction velocity $U_f = 0.067$ m s^{-1}, water depth $h = 6.4$ m, then $kh = 1.00$, $\epsilon = 0.06$ and $U_f/C = 0.01$. The preferred spacing between the surface streaks of the first unstable mode ($K = 2.7$) is 15 m according to the maximum growth rate in figure 10. The growth rate of this mode is about 0.004 s^{-1}, corresponding to the growth time of 250 s.

9. Longitudinal vortices in a wave-opposing current

Finally, we discuss the spanwise instability of a wave-opposing current (waves are from left to right; current is from right to left), which has a typical shear distribution shown in figure 12 for $h = 0.5$ m and $h = 3$ m, respectively. Note that shear rates in the basic current and in the wave-modified secondary current are both negative (opposite to the Stokes drift shear), hence are stabilizing.
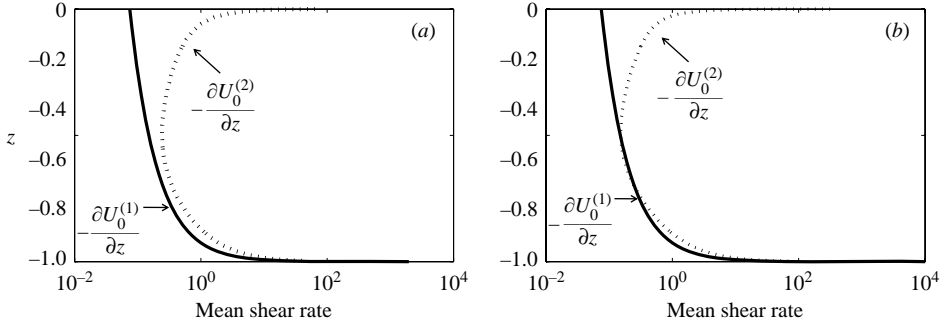
FIGURE 12. Typical shear rates of the the unperturbed current (dashed-line) and the perturbed current (solid line) in a wave-opposing current for $kh = 1$, $U_f/C = 0.003$, $\epsilon = 0.1$. (a) $h = 0.5$ m; (b) $h = 3$ m.

ϵ	σ_{st}	σ_{u_1}	σ_{u_2}	σ_{sw}	σ_ε	σ_r
5.00×10^{-2}	1.11×10^{-4}	-8.91×10^{-5}	-2.64×10^{-5}	2.48×10^{-2}	2.26×10^{-2}	2.13×10^{-3}
8.00×10^{-2}	1.12×10^{-4}	-6.39×10^{-5}	-3.86×10^{-5}	8.23×10^{-2}	6.96×10^{-2}	1.23×10^{-2}
1.20×10^{-1}	9.00×10^{-5}	-2.16×10^{-5}	-4.24×10^{-5}	1.99×10^{-1}	1.64×10^{-1}	3.34×10^{-2}

TABLE 6. Effect of wave slope on the energy budget of the first eigenmode in a wave-opposing current for $kh = 1$, $U_c/C = 0.003$, $K = 3$, $h = 3$ m.

The existence of the unstable modes has been examined in the manner of figure 3. For example, for the following inputs concerning waves and current: $kh = 1$, $U_f/C = 0.002$, $\epsilon = 0.05$, $K = 3$, and two depths $h = 0.5$ m and 3 m, only one unstable mode is found with the growth rates $\sigma_r = 0.022$ for $h = 0.5$ m and $\sigma_r = 0.023$ for $h = 3$ m. The principle of exchange of stability again holds.

We have also examined the growth rates σ_r of the first mode for the following inputs $kh = 1$, $U_f/C = 0.003$, $\epsilon \in [0.05, 0.12]$, $K \in [0.2, 8]$, for the water depth $h = 3$ m. The results are only slightly different from the case of wave-following current. Specifically, σ_r increases monotonically with increasing wave slope ϵ for any given transverse wavenumber K. For any wave slope, the growth rate increase monotonically with increasing K. There is no preferred transverse wavenumber.

The various contributions in the energy budget are the most revealing, as shown in table 6. For all wave slopes, σ_{sw} is comparable to σ_ε, while σ_{st} and σ_{u_2} are much smaller. In particular, both σ_{u_1} and σ_{u_2} associated with internal current shear are negative, and are stabilizing, as predicted by (1.1). However, with the wave-induced surface stress, an unstable mode is found in a wave-opposing current.

The typical eigenfunctions and cell pattern of the first mode have also been computed. As in the first unstable mode in a wave-following current, the vertical vorticity (or longitudinal velocity $\hat{u}_0$) does not change sign in the entire water depth. Thus, it is not surprising that the growth rate and the modal shapes of the unstable mode are similar to that of the wave-following current. Also omitted are the effects of kh and the curent strength, U_f/C; the results are similar to those of the wave-following current. We only mention that there is also a critical current strength above which there is no instability. For $kh = 1$, $\epsilon = 0.1$ and $h = 3$ m, this critical current strength is about $U_f/C = 0.0075$.

10. Concluding remarks

In this paper, a linearized theory for the instability of longitudinal vortices in water of finite depth has been presented. The current is assumed to be of the open-channel type with the characteristic velocity comparable to the wave orbital velocity. Turbulence generated by the current is described by a simple model of eddy viscosity. A key result is the apparent mean stress on the still water level, due to nonlinear interactions between wave oscillations and the steady current. This stress is non-zero even without wind, and contributes to the instability for longitudinal vortices. Although, in principle, unstable cells can occur in a wave-opposing current, it is in the wave-following current that the unstable cells (corresponding to the second mode) can be effective in vertical mixing and bringing up fine particles from the seabed.

When the Reynolds number is large, the eddy viscosity may be slightly different from that described by (2.1). The correction has been described by a wake funcition (Nezu & Rodi 1986). In Appendix D, we give numerical evidence that incorporating the wake function only leads to minor quantitative changes. Since the essential physics is easier to explain with the simple eddy viscosity model here, the wake function is not included in this work.

In addition to the obvious need for experiments in a wide tank, it is desirable to extend the present theory in several directions. An immediate next step is to predict the nonlinear evolution of the longitudinal vortices after the initial stage of instability. Finally, a full account of the interactions among wind, waves and Langmuir vortices in shallow water is a worthy challenge in hydrodynamics. With energy input from wind, waves may not attenuate in space. Possible coupling of the longitudinal vortices and nonlinear wave modulation (Benjamin–Feir instability) over a large spatial and temporal extent (x_2, t_2) may be important. These studies should be valuable for the prediction of suspension and transport of fine sediments in lakes and coastal seas.

Appendix A. Derivation of (4.29) and (4.30)

In (4.28), we look for terms linear in γ and independent of x and t. Since the eddy viscosity is of the order $O(\epsilon^2)$, the left-hand side of (4.28) is of the order $O(\gamma\epsilon^3)$. In order of appearance, the first term on the right-hand side is $O(\gamma\epsilon^5)$ since the integral is approximately $\overline{\eta[u]_0} \sim \overline{\epsilon H_1[\epsilon^2\gamma u_1]_0} = O(\gamma\epsilon^3)$. The second term is $O(\gamma\epsilon^6)$ since the integral is approximately $[\overline{\eta u^2}]_0 \sim [\overline{\epsilon H_1(\epsilon^2\gamma u_1)\epsilon U_0^{(1)}}]_0 = O(\gamma\epsilon^4)$. The third term is $O(\gamma\epsilon^3)$ since

$$\frac{\partial}{\partial y}\overline{\int_0^\eta (uv)\,\mathrm{d}z} \sim \frac{\partial}{\partial y}\overline{\eta[uv]_0} \sim \frac{\partial}{\partial y}\left[\overline{\epsilon H_1\epsilon U_1^{(1)}\epsilon\gamma v_0}\right]_0 = O(\gamma\epsilon^3), \qquad (\text{A }1)$$

where the fact that the primary wave is long-crested has been used. The fourth term is also $O(\gamma\epsilon^3)$ since

$$[uw]_0 \sim \left[\overline{(\gamma\epsilon^2 u_1)(\epsilon W_1^{(1)})} + \overline{(\gamma\epsilon^2 w_1)(\epsilon U_1^{(1)})}\right]_0 = O(\gamma\epsilon^3). \qquad (\text{A }2)$$

The fifth term is $O(\gamma\epsilon^5)$ since the pressure integral is approximately $[\overline{\eta p}]_0 \sim \overline{\epsilon H_1[\gamma\epsilon^2 p_1]_0} = O(\gamma\epsilon^3)$. In the sixth and seventh terms, we need contributions with

spanwise variations. The shear stress must be associated with the secondary waves so that τ_{xx}, τ_{xy} are of the order $O(\gamma\epsilon^4)$. The fifth term is $O(\gamma\epsilon^7)$ since the integral is $\overline{\eta[\tau_{xx}]_0} \sim O(\gamma\epsilon^5)$. For the same reason, the sixth term is $O(\gamma\epsilon^5)$. Finally, the eighth (last) term is proportional to

$$\epsilon^2 \frac{\partial}{\partial x_2}(\overline{\tilde{\eta}^2} + \overline{\eta}^2) \sim \epsilon^2 \frac{\partial}{\partial x_2}(\overline{\epsilon^2\gamma\eta_1\epsilon H_1} + \overline{\epsilon^2 H_0\epsilon^2\gamma\eta_0}) = O(\gamma\epsilon^5).$$

Use has been made of the fact the mean setdown is $\overline{H} = \epsilon^2 H_0$. Thus, the right-hand side of (4.28) is dominated by the third and fourth terms, as summarized in (4.29). Equation (4.30) follows by taking the time averages of the quadratic products shown in (A 1) and (A 2).

Appendix B. Numerical scheme for the wigenvalue problem

We solve numerically the eigenvalue problem stated in §5. To increase the numerical accuracy and avoid spurious modes, we work with equations (5.2)–(5.7) which are second-order differential equations. We first discretize the continuity and the momentum equations and then eliminate $\hat{G}_0$ and $\hat{v}_0$. The resulting numerical matrix equation is free of the spurious modes which would have arisen if we solved a higher-order system by first eliminating $\hat{G}_0$ and then making the discretization (see, e.g. Canuto *et al.* 1988).

The pseudospectral (PS) method (see, e.g. Gottlieb & Orszag 1977; Fornberg 1996, 1998; Boyd 2002) is used to approximate the vertical derivatives. Before applying the PS method, the vertical domain $z = [-kh + z_b, 0]$ is mapped linearly to $\xi = [-1, 1]$ by the linear transformation

$$z = -kh + z_b + \frac{kh - z_b}{2}(\xi + 1).$$

The derivatives in the ξ-coordinate are then discretized on a Chebyshev grid with nodes at $\xi_k = -\cos((k - 1)\pi/(N - 1))$, $k = 1, \ldots, N$, which are clustered near the two boundaries. The differentiation matrix described by Weideman & Reddy (2000) is employed. The treatment of the boundary conditions can be found in Fornberg (1998) and Boyd (2002).

Our algorithm has been validated in two ways. First, we used the numerical scheme to solve an inhomogeneous boundary-value problem similar to (5.2)–(5.7) except that all the coefficients (the shear rates and the eddy viscosity) are taken to be constants and a constant forcing term is added on the right-hand side of (5.4). For comparison, the same inhomogeneous problem was solved analytically by MAPLE 8 and numerically by the MATLAB routine bvp4c. To check the numerical resolution near $z = 0$, a very small $C_s = 10^{-6}$ was used. Indistinguishable results are obtained from the three methods. As a second test, we solved, by both MATLAB bvp4c and our pseudo-spectral method, another inhomogeneous boundary-value problem with constant shear rates, but variable eddy given by (2.5). Again, nearly identical answers are found to four-digit accuracy. For our eigenvalue problem, using 500 grid points in $\xi \in [0, 1]$ gives at least four-digit accuracy for the first four computed eigenvalues.

The dimensional bottom roughness z_B is an empirical parameter. If measured data are available, z_B can be obtained by fitting the measured velocity with the logarithmic profile. Otherwise, z_B can be determined from an empirical formula (see, e.g. Tennekes & Lumley 1972; Madsen & Wood 2002, etc.). In this paper, we adopt

from Madsen & Wood (2002) the following formula for a smooth bottom

$$z_b = kz_B = \frac{k\nu}{\mathcal{N}u_f},\tag{B 1}$$

where ν is the laminar kinetic viscosity, $\mathcal{N} = 9$, and u_f is the friction velocity of the turbulent current modified by waves. In view of the definitions of C_s and α, the dimensionless apparent bottom roughness z_b can be rewritten as

$$z_b = \frac{\kappa}{\mathcal{N}}\left(\frac{k\nu/C\epsilon^2}{\kappa u_f/C\epsilon^2}\right) = \frac{\kappa}{\mathcal{N}}\frac{C_s}{\alpha},\tag{B 2}$$

where both C_s and α must be computed based on the given wave and current conditions. For given water depth h and kh, the dimensional wave speed C can be computed from the dispersion relation, from which C_s can be computed for given wave slope ϵ. Typical values of C_s, z_b and α used in the present study are recorded in Appendix C.

In summary, the computational task involves the following steps. After prescribing the values of kh, U_f/C, ϵ, K, and the water depth h, we first solve for $U_0^{(2)}$ inside and outside the bottom wave boundary layer according to the two-dimensional theory of Huang & Mei (2003). In this process, parameters α and z_b are obtained. Then, the eigenvalue problem governed by (5.2)–(5.7) is solved, for a range of K to obtain the eigenvalues σ_2 and the eigenfunctions.

Appendix C. Typical input and output parameters

To show the range of input parameters used in the present study, we record below two typical cases.

Case 1. $h = 3$ m, $U_f/C = 0.004$, $kh = 1$.

ϵ	$C_s \times 10^{-6}$	$z_b \times 10^{-6}$	α_0	α	U_f/C	u_f/C
0.03	78.6	1.98	1.78	1.75	0.004	0.0039
0.05	28.2	2.0	0.64	0.62	0.004	0.0039
0.10	7.0	2.3	0.16	0.14	0.004	0.0034
0.15	3.1	2.83	0.07	0.049	0.004	0.0028

Case 2. $h = 0.5$ m, $U_f/C = 0.002$, $kh = 1$.

ϵ	$C_s \times 10^{-6}$	$z_b \times 10^{-6}$	α_0	α	U_f/C	u_f/C
0.03	1150.3	59.2	0.89	0.87	0.002	0.002
0.05	414.1	62.5	0.32	0.29	0.002	0.0018
0.10	103.5	85.0	0.08	0.055	0.002	0.0014
0.15	46.0	165.6	0.036	0.012	0.002	0.0007

Appendix D. Effects of the wake function

It is known from past experiments for uniform and steady open-channel flows that better fitting with data can be achieved by the following more complicated eddy
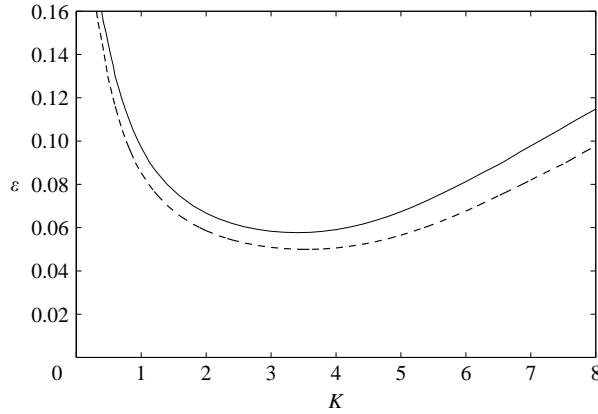
FIGURE 13. Effect of wake function on the marginal stability curve. Solid line: $\Pi = 0$; dashed-line: $\Pi = 0.2$. Other input parameters: $kh = 1.0$, $U_f/C = 0.003$ and $h = 3$ m.

viscosity,

$$\nu_T^* = \nu + \nu_e^*, \quad \nu_e^* = \frac{\kappa u_f(-z^*)\left(1 + \dfrac{z^*}{h}\right)}{1 + \pi\Pi\left(1 + \dfrac{z^*}{h}\right)\sin\left(\pi\left(1 + \dfrac{z^*}{h}\right)\right)}, \quad z_B^* - h < z^* < 0, \quad (\text{D}\,1)$$

where the denominator is called the wake function. Π is the empirical wake factor or Cole parameter (Nezu & Rodi 1986) which ranges from 0 to 0.2. Nezu & Rodi suggested that $\Pi = 0.2$ when the Reynolds number defined by water depth and mean velocity is larger than 10^5, which can be exceeded in water of $h = 0.5$ m and a mean velocity larger than 0.2 m s^{-1}. Note, however, that inclusion of the wake function causes only an $O(\Pi)$ reduction in the magnitude of the eddy viscosity at mid-depth and is of negligible consequence near the top and bottom boundaries where the shearing rates are large.

In an open-channel current with a wavy free surface, we replace the numerator of ν_e^* in (D 1) by $\kappa u_f(-z^* + \eta^*)(1 + z^*/h)$ so that the mixing length vanishes at the bottom and on the moving free surface (Van Duin & Janssen 1992; Huang & Mei 2003, etc.). Taking $\Pi = 0.2$, which is the largest empirical value suggested before, we have calculated the marginal stability curve, with and without the wake function, as compared in figure 13. It can be seen that the wake function yields a minor quantitative correction rendering the basic current slightly less unstable. Hence, the simpler model is chosen in this paper.

REFERENCES

BOYD, J. P. 2002 *Chebyshev and Fourier Spectral Methods*, 2nd edn. Dover.

CANUTO, C., HUSSAINI, M. Y., QUARTERONI, A. & ZANG, T. A. 1988 *Spectral Methods for Fluid Dynamics*. Springer.

CHANDRASEKHAR, S. 1961 *Hydrodynamic and Hydromagnetic Stability*. Dover.

CHINI, G. P. & LEIBOVICH, S. 2003 Resonant Langmuir-circulation internal-wave interaction. Part 1. Internal wave reflection. *J. Fluid Mech.* **495**, 35–55.

COX, S. M. & LEIBOVICH, S. 1993 Langmuir circulations in a surface layer bounded by a strong thermocline. *J. Phys. Oceanogr.* **23**, 1330–1345.

Cox, S. M. & Leibovich, S. 1994 Large-scale Langmuir circulation and double-diffusive convection: evolution equations and flow transitions. *J. Fluid Mech.* **276**, 189–210.

Cox, S. M. & Leibovich, S. 1997 Large-scale three dimensional Langmuir circulation. *Phys. Fluid* **9**, 2851–2863.

Craik, A. D. D. 1977 The generation of Langmuir circulations by an instability mechanism. *J. Fluid Mech.* **91**, 209–223.

Craik, A. D. D. 1982a The drift velocity of water waves. *J. Fluid Mech.* **116**, 187–205.

Craik, A. D. D. 1982b Wave-induced longitudinal-vortex instability in shear layer. *J. Fluid Mech.* **125**, 37–52.

Craik, A. D. D. & Leibovich, S. 1976 A rational model for Langmuir circulations. *J. Fluid Mech.* **73**, 401–426.

Dingemans, M.W., Kester, J. A. T. M. V., Radder, A. C. & Uittenbogaard, R. E. 1996 The effect of the CL-vortex force in 3d wave–current interaction. In *Coastal Engineering: Proc. 25th Intl Conf.* pp. 4821–4832. ASCE.

Faller, A. J. & Caponi, E. A. 1978 Laboratory studies of wind-driven Langmuir circulations. *J. Geophys. Res.* **83** (C7), 3617–3633.

Fornberg, B. 1996 *A Practical Guide to Pseudo-spectral Methods*. Cambridge University Press.

Fornberg, B. 1998 Calculation of weights in finite difference formulas. *SIAM Rev.* **40**, 685–691.

Gnanadesikan, A. 1996 Mixing driven by vertically variable forcing: an application to the case of Langmuir circulation. *J. Fluid Mech.* **322**, 81–107.

Gottlieb, D. & Orszag, S. A. 1977 *Numerical Analysis of Spectral Methods: Theory and Applications*. SIAM.

Graham, A. & Hall, A. J. 1997 The horizontal distribution of bubbles in a shallow sea. *Continental Shelf Research* **17**, 1051–1082.

Grant, W. D. & Madsen, O. S. 1986 The continental-shelf bottom boundary layer. *Annu. Rev. Fluid Mech.* **18**, 265–305.

Groeneweg, J. & Battjes, J. A. 2003 Three-dimensional wave effects on a steady current. *J. Fluid Mech.* **478**, 325–343.

Groeneweg, J. & Klopman, G. 1998 Change of the mean velocity profiles in the combined wave–current motion described in a GLM formulation. *J. Fluid Mech.* **370**, 271–296.

Hall, P. & Smith, F. T. 1988 The nonlinear interaction of Tollmien–Schlichting waves and Taylor-Gortler vortices in curved channel flows. *Proc. R. Soc. Lond.* A **417**, 255–282.

Huang, Z. & Mei, C. C. 2003 Effects of surface waves on a turbulent current over a smooth or rough seabed. *J. Fluid Mech.* **497**, 253–287.

Kajiura, K. 1968 A model of the bottom boundary layer in water waves. *Bull. Earthquake Res. Institute* **46**, pp. 75–123.

Kemp, P. H. & Simons, R. R. 1982 The interaction between waves and a turbulent current: waves propagating with the current. *J. Fliud Mech.* **116**, 227–250.

Kemp, P. H. & Simons, R. R. 1983 The interaction between waves and a turbulent current: waves propagating against the current. *J. Fliud Mech.* **130**, 73–89.

Klopman, G. 1997 Secondary circulation of the flow due to waves and current: laser-Doppler flow measurements for waves following or opposing a current. *Tech. Rep.* Z2249. Delft Hydraulics.

Langmuir, I. 1938 Surface motion of water induced by wind. *Science* **87**, 119–123.

Leibovich, S. 1977a System of wind drift currents and Langmuir circulations in the ocean. *J. Fluid Mech.* **79**, 715–743.

Leibovich, S. 1977b Convective instability of stably stratified water in the ocean. *J. Fluid Mech.* **82**, 561–585.

Leibovich, S. 1983 The form and dynamics of Langmuir circulation. *Annu. Rev. Fluid Mech.* **15**, 391–427.

Leibovich, S. & Paolucci, S. 1981 The instability of the ocean to Langmuir circulation. *J. Fluid Mech.* **102**, 141–167.

Leibovich, S. & Radhakrishnan, K. 1977 On the evolution of the system of wind drift currents and Langmuir circulations in the ocean. Part 2. Structure of the Langmuir vortices. *J. Fluid Mech.* **80**, 481–507.

Li, M. & Garrett, C. 1997 Mixed layer deepening due to Langmuir circulation. *J. Phys. Oceanogr.* **27**, 121–132.

LI, M., ZAHARIEV, K. & GARRETT, C. 1995 Role of Langmuir circulation in the deepening of the ocean surface mixed layer. *Science* **270**, 1955–1957.

LIU, A.-K. & DAVIS, S. H. 1977 Viscous attenuation of mean drift in water waves. *J. Fluid Mech.* **81**, 63–84.

LONGUET-HIGGINS, M. S. 1953 Mass transport in water waves. *Phil. Trans. R. Soc. Lond.* A **245**, 535–581.

MADSEN, O. S. & WOOD, W. 2002 Sediment transport outside the surf zone. In *Coastal Engineering Manual–Part III*. US Army Corps of Engineers.

MATHISEN, P. P. & MADSEN, O. S. 1996 Waves and currents over a fixed rippled bed 1. Bottom roughness experienced by waves in the presence and absence of currents. *J. Geophys. Res.* **101**(C7), 16533–16542.

MEI, C. C. 1989 *The Applied Dynamics of Ocean Surface Waves*, 2nd edn. World Scientific.

MELVILLE, W. K., SHEAR, R. & VERON, F. 1998 Laboratory measurements of the generation and evolution of Langmuir circulation. *J. Fluid Mech.* **364**, 31–58.

NEPF, H. M., COWEN, E. A., KIMMEL, S. J. & MONISMITH, S. G. 1995 Longitudinal vortices beneath breaking waves. *J. Geophys. Res.* **100** (C8), 16211–16221.

NEPF, H. M. & MONISMITH, S. G. 1991 Experimental study of wave-induced longitudinal vortices. *J. Hydraul. Engng* **117**, 1639–1649.

NEZU, I. & RODI, W. 1986 Open-channel flow measurements with a laser doppler anemometer. *J. Hydraul. Engng* **112**, 335–355.

PHILLIPS, O. M. 1977 *The Dynamics of the Upper Ocean*, 2nd edn. Cambridge University Press.

PHILLIPS, W. R. C. 1998 Finite-amplitude rotational waves in viscous shear flows. *Stud. Appl. Maths* **101**, 23–47.

PHILLIPS, W. R. C. 2001 On an instability to Langmuir circulations and the role of Prandtl and Richardson numbers. *J. Fluid Mech.* **442**, 335–358.

PHILLIPS, W. R. C. 2002 Langmuir circulations beneath growing or decaying surface waves. *J. Fluid Mech.* **469**, 317–342.

SKYLLINGSTAD, E. D. & DENBO, D. W. 1995 An ocean large-eddy simulation of Langmuir circulation and convection in the surface layer. *J. Geophys. Res.* **100** (C5), 8501–8522.

SMITH, J. A. 1992 Observed growth of Langmuir circulation. *J. Geophys. Res* **97** (C4), 5651–5664.

SMITH, J. A., PINKEL, R. & WELLER, R. A. 1987 Velocity fields in the mixed layer during MILDEX. *J. Phys. Oceanogr.* **17**, 425–439.

SZERI, A. J. 1996 Langmuir circulations on Rodeo Lagoon. *Mon. Weather Rev.* **124**, 341–342.

TENNEKES, H. & LUMLEY, J. L. 1972 *A First Course in Turbulence*. The MIT Press.

THORPE, S. A. 2004 Langmuir circulation. *Annu. Rev. Fluid Mech.* **36**, 55–79.

TOWNSEND, A. A. 1972 Flow in a deep turbulent boundary layer over a surface distorted by water waves. *J. Fluid Mech.* **55**, 719–735.

VAN DUIN, C. A. & JANSSEN, P. A. E. M. 1992 An analytical model of the generation of surface waves by turbulent air flow. *J. Fluid Mech.* **236**, 197–215.

WEIDEMAN, J. A. C. & REDDY, S. C. 2000 A Matlab differentiation matrix suite. *ACM TOMS* **26**, 465–519.

WELLER, R. A., DEAN, J. P., MARRA, J., PRICE, J. F., FRANCIS, E. A. & BOARDMAN, D. C. 1985 Three dimensional flow in the upper ocean. *Science* **227**, 1552–1556.

WELLER, R. A. & PRICE, J. F 1988 Langmuir circulation within the ocanic mixed layer. *Deep-sea Res.* **35**, 711–747.